

# Journal Pre-proof

Multiplex HDR for Disease and Correction Modeling of SCID by CRISPR Genome Editing in Human HSPCs

Ortal Iancu, Daniel Allen, Orli Knop, Yonathan Zehavi, Dor Breier, Adaya Arbiv, Atar Lev, Yu Nee Lee, Katia Beider, Arnon Nagler, Raz Somech, Ayal Hendel

PII: S2162-2531(22)00323-7

DOI: <https://doi.org/10.1016/j.omtn.2022.12.006>

Reference: OMTN 1792

To appear in: *Molecular Therapy: Nucleic Acid*

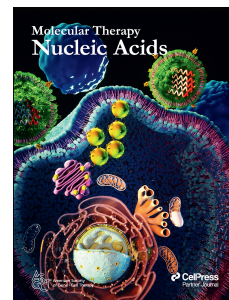
Received Date: 18 May 2022

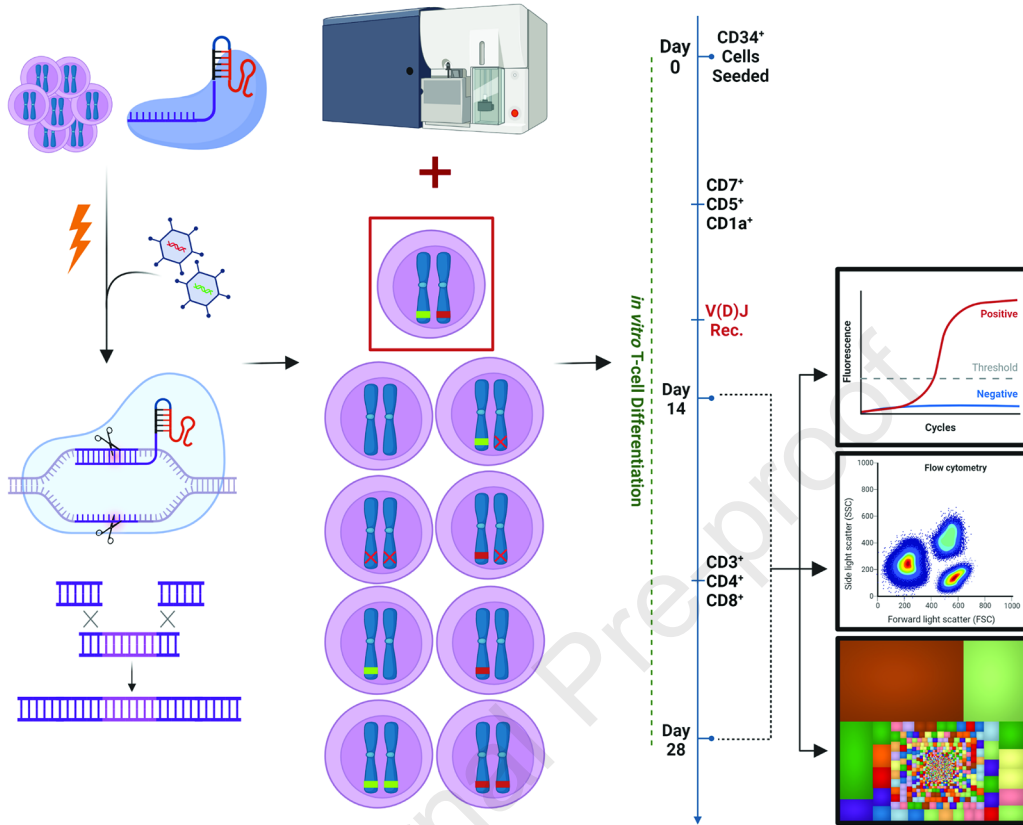
Accepted Date: 7 December 2022

Please cite this article as: Iancu O, Allen D, Knop O, Zehavi Y, Breier D, Arbiv A, Lev A, Lee YN, Beider K, Nagler A, Somech R, Hendel A, Multiplex HDR for Disease and Correction Modeling of SCID by CRISPR Genome Editing in Human HSPCs, *Molecular Therapy: Nucleic Acid* (2023), doi: <https://doi.org/10.1016/j.omtn.2022.12.006>.

This is a PDF file of an article that has undergone enhancements after acceptance, such as the addition of a cover page and metadata, and formatting for readability, but it is not yet the definitive version of record. This version will undergo additional copyediting, typesetting and review before it is published in its final form, but we are providing this version to give early visibility of the article. Please note that, during the production process, errors may be discovered which could affect the content, and all legal disclaimers that apply to the journal pertain.

© 2022 The Author(s).





1 **Multiplex HDR for Disease and Correction Modeling of SCID by CRISPR Genome Editing**  
2 **in Human HSPCs**

3

4 Ortal Iancu<sup>1#</sup>, Daniel Allen<sup>1#</sup>, Orli Knop<sup>1#</sup>, Yonathan Zehavi<sup>1</sup>, Dor Breier<sup>1</sup>, Adaya Arbiv<sup>1</sup>, Atar  
5 Lev<sup>1,2</sup>, Yu Nee Lee<sup>2,3</sup>, Katia Beider<sup>4</sup>, Arnon Nagler<sup>3,4</sup>, Raz Somech<sup>2,3</sup>, and Ayal Hendel<sup>1\*</sup>

6

7 1. The Institute for Advanced Materials and Nanotechnology, The Mina and Everard  
8 Goodman Faculty of Life Sciences, Bar-Ilan University, Ramat Gan, 5290002, Israel

9 2. Pediatric Department A and the Immunology Service, Jeffrey Modell Foundation Center,  
10 Edmond and Lily Safra Children's Hospital, Sheba Medical Center, Tel-HaShomer, Ramat  
11 Gan, 5266202, Israel

12 3. Sackler Faculty of Medicine, Tel Aviv University, Tel Aviv, 6997801, Israel

13 4. The Division of Hematology and Bone Marrow Transplantation, Chaim Sheba Medical  
14 Center, Tel-HaShomer, Ramat Gan, 5266202, Israel

15 \* *Correspondence should be addressed to A.H. (Ayal.hendel@biu.ac.il):*

16 Bar-Ilan University, Ramat-Gan, 5290002, Israel

17 Tel: +972-3-5317316

18 # These authors contributed equally to this work

19 Running title: CRISPR-Cas9/rAAV6 Genome Editing for Modeling and Correction of  
20 SCID Disease

## 21 Abstract

22 Severe combined immunodeficiency (SCID) is a group of disorders caused by mutations in genes  
23 involved in the process of lymphocyte maturation and function. CRISPR-Cas9 gene editing of the  
24 patient's own hematopoietic stem and progenitor cells (HSPCs) *ex vivo* could provide a therapeutic  
25 alternative to allogeneic hematopoietic stem cell transplantation (HSCT), the current gold standard  
26 for treatment of SCID. In order to eliminate the need for scarce patient samples, we engineered  
27 genotypes in healthy donor (HD)-derived CD34<sup>+</sup> HSPCs using CRISPR-Cas9/rAAV6 gene-  
28 editing, to model both SCID and the therapeutic outcomes of gene-editing therapies for SCID via  
29 multiplexed homology directed repair (HDR). Firstly, we developed a SCID disease model via  
30 biallelic *knock-out* of genes critical to the development of lymphocytes; and secondly, we  
31 established a *knock-in/knock-out (KI-KO)* strategy to develop a proof-of-concept single-allelic  
32 gene correction. Based on these results, we performed gene correction of RAG2-SCID patient-  
33 derived CD34<sup>+</sup> HSPCs that successfully developed into CD3<sup>+</sup> T cells with diverse TCR repertoires  
34 in an *in-vitro* T-cell differentiation (IVTD) platform. In summary, we present a strategy to  
35 determine the optimal configuration for CRISPR-Cas9 gene correction of SCID using HD-derived  
36 CD34<sup>+</sup> HSPCs, and the feasibility of translating this gene-correction approach in patient-derived  
37 CD34<sup>+</sup> HSPCs.

## 38 Introduction

39 Severe combined immunodeficiency (SCID) is a group of multiple monogenic disorders  
40 characterized by a profound block of T-cell development that harms both cellular and humoral  
41 adaptive immunity.<sup>1,2</sup> Depending on the type of SCID, B and NK cells may also be affected. Thus,  
42 based on the affected gene, patients can be classified according to the presence or absence of T, B,

43 and NK lymphocytes (T-, B-/+, and NK-/+, respectively). The most common SCID is X-linked  
44 SCID (SCID-X1 [from mutations in the *IL2RG* gene]), which presents with a T-B+NK- immune  
45 phenotype. Other forms of SCID can develop as a result of mutations in *Recombination-activating*  
46 *gene 1* (*RAG1*), *RAG2*, or *DNA Cross-Link Repair 1C* (*DCLRE1C*) and display the T-B-NK+  
47 immune phenotype, while other forms develop from mutations in the *Interleukin 7 Receptor*  
48 *Subunit Alpha* (*IL7RA*) gene and present with a T-B+NK+ immune phenotype.<sup>3-7</sup> *RAG1* and *RAG2*  
49 genes encode proteins that, when complexed together, commence the lymphoid-specific variable  
50 (V), diversity (D), and joining (J) gene [V(D)J] recombination process by catalyzing DNA double-  
51 strand breaks (DSBs) at the recombination signal sequences (RSSs) which flank the V, D, and J  
52 gene segments.<sup>8</sup> The *DCLRE1C* gene encodes the Artemis protein which assists in the functional  
53 resection of the V, D, and J gene segments by employing its endonuclease activity on the 5' and 3'  
54 overhangs and hairpins of the RAG-complex-induced DSBs.<sup>9</sup> V(D)J recombination is a critical  
55 step in the maturation of T and B cells as it is responsible for the generation of a diverse repertoire  
56 of T and B cell receptors (TCR and BCR, respectively).<sup>10</sup> Thus, patients with disease-causing  
57 variants in the *RAG1*, *RAG2*, or *DCLRE1C* genes typically present with significantly reduced or  
58 complete absence of T and B cells. *IL7RA* signaling plays a major role at various stages of T-cell  
59 development, namely ensuring the survival of naive T cells and assisting in the homeostatic  
60 expansion of both naive and memory T cells via proliferation.<sup>11</sup> Thus, typical patients with  
61 mutations in the *IL7RA* gene will present a lack of T cells. Ineffective expression of any of these  
62 genes can lead to SCID, highlighted by severe lymphopenia and lack of cellular and humoral  
63 adaptive immunity.<sup>6</sup>

64 Infants born with SCID appear healthy in the first few weeks of life, however, following  
65 environmental exposure to pathogens and the decline of maternally transferred antibodies, they

66 become prone to develop life-threatening bacterial, viral, and/or fungal infections. Without early  
67 intervention to reconstitute their immune system, patients often do not survive past the first two  
68 years of life.<sup>2</sup> The definitive curable treatment for SCID patients is allogeneic HSCT from a human  
69 leukocyte antigen (HLA)-matched (related or unrelated) donor.<sup>12</sup> If a full HLA-matched donor is  
70 not available, patients may undergo haploidentical HSCT from one of their parents. Successful  
71 HSCT promotes lymphoid lineage development resulting in a long-term patient survival rate of  
72 >80%, however, there are significant limitations to this approach especially in the absence of a  
73 HLA-matched donor where the survival rate decreases to 60-70%.<sup>13,14</sup> These limitations include  
74 graft failure after HSCT that leads to poor immune reconstitution as well as potentially fatal graft-  
75 versus-host disease (GvHD).<sup>15,16</sup> Therefore, due to the devastating nature of SCID and the  
76 limitations of HSCT, it is crucial to develop new treatment options, such as gene therapy.

77 The ability to genetically edit CD34<sup>+</sup> hematopoietic stem and progenitor cells (HSPCs) as well as  
78 the cells' marked ability to reconstitute the immune system from a small number of original cells,  
79 make these stem cells an attractive target for gene therapy.<sup>17,18</sup> Viral vectors can facilitate the  
80 delivery of a corrected transgene to autologous HSPCs *ex vivo* as was previously established in  
81 gene therapy clinical trials using lentiviral (LV) or gammaretroviral ( $\gamma$ RV) transduction.<sup>19,20,21-23</sup>  
82 Treatment of Chronic Granulomatous Disease (CGD), Wiskott-Aldrich Syndrome (WAS), SCID-  
83 X1, and most recently of Adenosine Deaminase (ADA)-SCID with  $\gamma$ RV resulted in the activation  
84 of proto-oncogenes leading to a leukemic transformation in some patients.<sup>24-29</sup> To improve the  
85 safety of viral transgene delivery, LVs have replaced  $\gamma$ RVs, the viral enhancer sequences  
86 responsible for the elevated risk of genotoxicity were removed, and a self-inactivating element  
87 was added to the vectors.<sup>30</sup> This resulted in successful therapy for SCID-X1 patients, however,  
88 expansion of a single clonal population was reported in one patient case.<sup>31-34</sup> The main

89 disadvantages of using  $\gamma$ RV and LV vectors for CD34<sup>+</sup> HSPC gene therapy remain the semi-  
90 random integration and constitutive expression of the transgene which can lead to incomplete  
91 phenotypic correction, dysregulated hematopoiesis, toxicity, and insertional mutagenesis.<sup>35</sup> Thus,  
92 delivery of the transgene via a targeted genome-editing approach could prove beneficial.

93 Clustered regularly interspaced short palindromic repeats (CRISPR) and CRISPR-associated  
94 nuclease 9 (Cas9), commonly known as CRISPR-Cas9, has had a tremendous impact on the field  
95 of gene editing due to its simplicity, specificity, and applicability in a wide variety of cell types.<sup>36-</sup>  
96 <sup>38</sup> The combination of CRISPR-Cas9 and a donor DNA molecule delivered by recombinant adeno-  
97 associated virus serotype 6 (rAAV6) can provide a therapeutic approach to genome editing in  
98 CD34<sup>+</sup> HSPCs. Although rAAV6 lacks any integration machinery of its own, precise targeting and  
99 insertion of the donor DNA payload through the homology-directed repair (HDR) pathway in  
100 CD34<sup>+</sup> HSPCs can occur following the Cas9-induced site-specific DSB.<sup>39-41</sup> However, the use of  
101 rAAV6 vectors is not without challenges. Our group has shown that rAAV6 vectors are recognized  
102 by cellular repair proteins triggering a DNA damage response (DDR) proportional to that of the  
103 amount of virus used, referred to as the multiplicity of infection (MOI).<sup>42</sup> Therefore, when  
104 developing rAAV6-based protocols, reducing the MOI as much as possible, while maintaining the  
105 required levels of HDR, is of utmost importance.

106 Developing a gene-therapy strategy requires a thorough understanding of the disease phenotype  
107 and extensive assessment of the viability of the respective functional gene correction before it can  
108 reach the clinic. To achieve this, large amounts of patient samples are required to model and test  
109 the method *ex vivo*. Since SCID patients are infants, neither drawing large amounts of peripheral  
110 blood (PB) nor retrieving large samples through invasive bone-marrow procedures are viable  
111 options for procuring such samples for pre-clinical proof-of-concept research. Therefore, obtaining

112 sufficient amounts of SCID patient-derived CD34<sup>+</sup> HSPCs presents a major challenge. To  
113 circumvent the need for large amounts of patient samples, we utilized multiplex HDR, which has  
114 been shown to be an effective method for the enrichment of cells with engineered genotypes.<sup>43</sup> We  
115 engineered HD-derived CD34<sup>+</sup> HSPCs to (1) model SCID and (2) simulate gene-correction  
116 therapies for SCID. Via cell sorting, we were then able to enrich for cells with the desired  
117 engineered genotype to model and track their T-cell progression.

118 In this study, we accomplished three main goals towards bringing a curative gene therapy for SCID  
119 closer to becoming a reality, while providing a more general technique for modeling other  
120 recessive blood disorders using HD-derived CD34<sup>+</sup> HSPCs. (1) We developed an innovative  
121 autosomal recessive SCID disease model via biallelic *knock-out (KO)* of *RAG2*, *DCLRE1C*, or  
122 *IL7RA* genes in HD-derived CD34<sup>+</sup> HSPCs. When *KO* CD34<sup>+</sup> HSPCs were subjected to a stromal  
123 cell-free, IVTD system,<sup>44</sup> these engineered cells lacked the ability to differentiate into CD3-  
124 expressing cells and presented a failure in execution of TCR V(D)J recombination, similar to that  
125 of SCID-patient-derived cells. (2) We then utilized a *KI-KO* approach to simulate functional gene  
126 correction of *RAG2* in HD-derived CD34<sup>+</sup> HSPCs. Due to the recessive nature of SCID, correction  
127 of only one allele is sufficient to cure the patient. In this strategy, we mimicked monoallelic  
128 correction in SCID-patient cells by *knock-in (KI)* of a codon-optimized diverged cDNA cassette  
129 into the endogenous *RAG2* loci in one allele (thereby preserving regulatory non-coding elements)  
130 and *KO* of the second allele. In contrast to the *RAG2* biallelic *KO* cells, the *KI-KO* differentiated  
131 T cells presented normal CD3 expression and TCR repertoire diversity. (3) Lastly, we showed  
132 first-of-its-kind functional gene correction of *RAG2*-SCID patient-derived CD34<sup>+</sup> HSPCs. In  
133 contrast to the unedited *RAG2*-SCID-patient cells, the corrected population developed into CD3<sup>+</sup>  
134 T cells with diverse TCR repertoires. Overall, our method provides a platform to study the disease

135 phenotypes with a multi-parameter readout in the form of immunophenotyping and V(D)J  
136 recombination assessment via next-generation sequencing (NGS) and will allow researchers to  
137 determine the optimal configuration for gene therapies for other SCIDs and immunodeficiencies.

## 138 **Results**

### 139 **Modeling SCID disease with CRISPR-Cas9/rAAV6-mediated biallelic *KO* in HD-derived** 140 **CD34<sup>+</sup> HSPCs**

141 In order to generate biallelic *KO* of the *RAG2*, *DCLRE1C*, or *IL7RA* genes individually in HD-  
142 derived CD34<sup>+</sup> HPSCs, chemically modified sgRNAs were designed to target the genomic DNA  
143 a few base-pairs downstream of the respective gene's start codon.<sup>37</sup> We PCR amplified each  
144 individual gene's on-target site and quantified the INDEL frequencies of the corresponding Sanger  
145 sequences via the tracking of INDELS by decomposition (TIDE) analysis and found that all  
146 sgRNAs induced INDELS at high frequencies yet produced distinctly different INDEL patterns  
147 (Figure S1A-E). Additionally, we used NGS to map the INDEL events of the *RAG2* sgRNA and  
148 found that the distinct pattern was highly reproducible (Figure S1F).

149 The sgRNA was delivered together with the Cas9 endonuclease as a ribonucleoprotein (RNP)  
150 complex in conjunction with rAAV6 vectors carrying a DNA template for gene disruption. The  
151 template contained a reporter gene flanked by arms of homology for HDR at the aforementioned  
152 CRISPR-Cas9 cut-site. Following successful HDR, the integration of the reporter gene into the  
153 target gene's open reading frame was expected to abolish the transcription of the coding region of  
154 the target gene (Figure 1A). Two DNA donors, each containing a distinct reporter gene, were  
155 required for each gene to allow for multiplex HDR and biallelic *KO* enrichment via cell sorting of  
156 cells expressing both reporter genes. We used two control groups in the following analyses: (1)

157 cells electroporated without the presence of the RNP complex or rAAV6 (herein referred to as  
158 *Mock*) as well as (2) cells with biallelic *KO* of the *C-C motif chemokine receptor 5 (CCR5)* gene.  
159 While *CCR5* is expressed in T cells, its expression does not affect T-cell development, allowing  
160 for the determination of the effect of CRISPR-Cas9 and rAAV6 treatments on the T-cell  
161 developmental process. Biallelic targeting of *RAG2* and *CCR5* was carried out with green  
162 fluorescent protein (GFP) and truncated nerve growth factor receptor (tNGFR) reporter genes  
163 (Figure 1A and S2A), whereas biallelic targeting of *DCLRE1C* and *IL7RA* were carried out with  
164 GFP and tdTomato reporter genes (Figure S2B and S2C). Immediately following electroporation,  
165 cells were exposed to their respective rAAV6 donors. Two days post-electroporation, the cells  
166 were sorted for CD34 expression, and double-positive reporter gene expression tNGFR<sup>+</sup>/GFP<sup>+</sup> or  
167 tdTomato<sup>+</sup>/GFP<sup>+</sup>, indicative of biallelic *KO* (See example for *RAG2* in Figure 1B). Average  
168 biallelic HDR frequencies at the different loci ranged from 1.7-4.6% (Figure 1C and S2D). DNA  
169 was purified from cells that were cultured in CD34<sup>+</sup> HSPCs medium post-sort and the DNA was  
170 analyzed by Digital Droplet PCR (ddPCR) for quantification of locus-specific target integration.  
171 ddPCR analysis revealed that the *CCR5*, *RAG2*, and *DCLRE1C* sorted cells contained the *KO*  
172 disruption DNA donors in ~100% of the alleles whereas *IL7RA* sorted cells showed slightly less  
173 efficient integration (Figure S2E).

#### 174 **Modeled SCID CD34<sup>+</sup> HSPCs do not progress to CD3<sup>+</sup> T Cells in a cell-free *in-vitro* T-cell** 175 **differentiation system**

176 CD34<sup>+</sup> HSPCs differentiate into CD7<sup>+</sup>/CD5<sup>+</sup> pro-T cells which then continue to develop into T-  
177 cell-committed pre-T CD1a<sup>+</sup> cells (identifiable in IVTD by immunostaining on day 14). These  
178 CD7<sup>+</sup>/CD1a<sup>+</sup> cells can then undergo TCR rearrangement and become immature single-positive  
179 (ISP) CD4<sup>+</sup> T cells. These give rise to double-positive (DP) CD4<sup>+</sup>/CD8<sup>+</sup> cells that express CD3

180 (identifiable in IVTD by immunostaining on day 28 and 42 [in cases where extensive follow-up is  
181 required]). These cells then undergo full maturation into CD3-expressing single-positive (SP)  
182 CD8<sup>+</sup> or CD4<sup>+</sup> cells (i.e., CD3<sup>+</sup>/CD8<sup>+</sup> or CD3<sup>+</sup>/CD4<sup>+</sup> cells [Figure S3A]). CD3 receptors form a  
183 complex with the cell's TCR, which serves a fundamental role in the maturation of thymocytes  
184 from their immature precursors. Typical SCID is characterized by the absence of or significant  
185 reduction in CD3<sup>+</sup> T cells (<300 cells/ml).<sup>45</sup> The stromal cell-free IVTD system that we used  
186 provided the ability for easy observation and immunophenotyping by flow cytometry of T-cell  
187 development at predetermined time points and assessment of V(D)J recombination via NGS  
188 analysis.

189 In order to model *RAG2*-, *DCLRE1C*-, or *IL7RA*-SCID, biallelic KO CD34<sup>+</sup> HSPCs for each locus  
190 were individually cultured in the IVTD system and compared to *Mock* and *CCR5* KO populations.  
191 Consistent with the literature, the *IL7RA* biallelic KO populations presented complete cell death  
192 after only 6 days in culture (Figure 2A), whereas cells that had no HDR integration were  
193 predominantly viable cells (Figure S3B).<sup>6</sup> In contrast, *Mock* cells and *CCR5*, *RAG2*, and  
194 *DCLRE1C* biallelic KO populations were able to proliferate through the 28 day time point (Figure  
195 2B). Immunophenotyping by flow cytometry revealed no significant difference in the expression  
196 levels of CD5, CD7, or CD1a between the *RAG2* or *DCLRE1C* KO and *CCR5* KO cells after 14  
197 days. Additionally, similar expression of both CD4 and CD8 was observed in all three groups after  
198 28 days. However, at this stage of differentiation, *CCR5* KO cells developed into CD3<sup>+</sup> T cells,  
199 while hardly any *RAG2* or *DCLRE1C* KO cells expressed CD3 (Figure 2B and S3C). Furthermore,  
200 as expected, the expression of the endogenous *RAG2* and *DCLRE1C* genes were drastically  
201 reduced in the *RAG2* and *DCLRE1C* biallelic KO populations (Figure S3D-E).

202 Due to their central role in somatic recombination, we sought to determine whether the *RAG2* and  
203 *DCLRE1C* KO cells were able to perform functional V(D)J recombination, the lack of which is a  
204 hallmark of SCID lymphocytes. To do so, we deep-sequenced the T-cell receptor gamma (TRG)  
205 loci, one of the first chains to be recombined among the different TCR chains.<sup>46,47</sup> Preparation of  
206 TRG libraries from *RAG2* KO cells revealed no amplification of the recombined locus (Figure  
207 S3F) and the rearrangement in *DCLRE1C* KO cells was similarly impaired, noted by standard PCR  
208 amplification using primers flanking the V-J regions of the TRG locus (Figure S3G). Taken  
209 together, our IVTD approach can be used to accurately model SCID and help us characterize the  
210 SCID phenotype for validation of future gene-correction results. This was highlighted by  
211 accurately producing the gene-specific disease phenotypes: *IL7RA* KO cells did not proliferate or  
212 differentiate at all and *DCLRE1C* KO and *RAG2* KO cells neither developed into CD3<sup>+</sup> T cells nor  
213 underwent effective TCR V(D)J recombination.

#### 214 **T-cell differentiation phenotype of SCID-patient cells validates the disease model**

215 To validate our use of the IVTD platform as a reliable method to model the SCID phenotype, we  
216 subjected SCID-patient-derived CD34<sup>+</sup> HSPCs to 42 days of IVTD and examined their  
217 differentiation capability (Figure S4A). The SCID-patient-derived CD34<sup>+</sup> HSPCs samples were  
218 extracted and purified from the PB of *RAG1*- and *RAG2*-SCID patients (Figure S4B-C). Both  
219 patients presented with a clinical phenotype suggestive of SCID and subsequent immune workup  
220 and genetic testing confirmed the diagnosis. The first patient is homozygous for a 4bp deletion  
221 (c.1407-10 del.4bp-TTGC) in the *RAG1* gene, resulting in a frameshift mutation, premature stop  
222 codon, and dysfunctional RAG1 protein, while the second patient is homozygous for a missense  
223 mutation (c.G104T; p.G35V) in the *RAG2* gene, which reduces the binding capabilities of RAG2

224 to RAG1 during V(D)J recombination.<sup>8,48</sup> Alongside the CD34<sup>+</sup> HSPCs from each patient, control  
225 HD-derived PB CD34<sup>+</sup> HSPCs were seeded in the IVTD system.

226 After 14 days, there was no significant immunophenotypic difference in CD5 or CD7 expression  
227 between the groups, however, a range of CD1a expression was noticed across the sample  
228 populations (0-37%) (Figure S4A). Following 28 and 42 days in the IVTD system, the SCID-  
229 patient-derived cells did not differentiate into CD3<sup>+</sup> cells and cell viability was still >90% in all  
230 samples, indicative of a halt in T-cell progression (Figure S4A). To emphasize the V(D)J  
231 recombination impairment in the SCID-patient cells compared to the HD-derived PB control, DNA  
232 was extracted and used as a template for TRG recombination PCR. The HD-derived PB cells  
233 successfully underwent TRG recombination, whereas the SCID-patient-derived PB cells failed  
234 (Figure S4D-F). An additional sample of cells was extracted and purified from PB of the *RAG1*-  
235 SCID patient following successful HSCT and subjected to the IVTD system. Consistent with the  
236 clinical reports, the *RAG1*-SCID cells post-HSCT showed robust CD3 expression (Figure S4A and  
237 Table S1) and completed successful TRG V(D)J recombination by day 14 (Figure S4F).

### 238 **Biallelic *KI-KO* targeting of *RAG2* in HD-derived CD34<sup>+</sup> HSPCs to simulate functional gene** 239 **correction**

240 Since *RAG2*-SCID is an autosomal recessive disorder, correction of only one allele is required to  
241 have the patient develop a functional immune system. This is highlighted by the fact that carriers  
242 of *RAG2* mutations (e.g., the parents of the *RAG2*-SCID patient) present as fully healthy  
243 individuals. We aimed to utilize multiplex HDR for *RAG2 KI-KO* for correction simulation in HD-  
244 derived CD34<sup>+</sup> HSPCs. This provided three main advantages over alternative editing strategies  
245 which requires prolonged culturing of the cells and can be done using induced pluripotent stem

246 cells (iPSCs) (e.g. first actuate *RAG2 KO* and then subsequently correct the previously *KO* cells).  
247 (1) In contrast to prior works that have used iPSCs, HD-derived CD34<sup>+</sup> HSPCs provided us with  
248 the capability of using biologically-authentic CD34<sup>+</sup> HSPCs, the same cells that are used in  
249 HSCT<sup>49</sup>; (2) Culturing CD34<sup>+</sup> HSPCs for too long reduces the cells regenerative potential. CD34<sup>+</sup>  
250 HSPCs maintain their stemness and a balance between proliferation, quiescence, and regeneration  
251 as well as their ability to differentiate to all hematopoietic cell lineages for a limited time in culture.  
252 Extensive culturing protocols with multiple editing steps have been shown to lead to a loss of the  
253 stem cells qualities and engraftment potential in murine models;<sup>50</sup> and (3) It provides the ability to  
254 circumvent the need for scarce patient samples to establish the feasibility of our correction strategy.

255 Based on this, we aimed to simulate functional gene correction of *RAG2* in HD-derived CD34<sup>+</sup>  
256 HSPCs via multiplex HDR using two distinct rAAV6 donors to actuate biallelic *KI-KO*. In the  
257 HD-derived CD34<sup>+</sup> HSPCs, we targeted one allele with a *KI* template containing diverged  
258 functional *RAG2* cDNA (along with a [tNGFR] reporter gene cassette under the regulation of a  
259 constitutive phosphoglycerokinase (PGK) promoter) (Figure 3A) and the other allele with a *KO*  
260 template consisting of a disrupting reporter cassette (*KO* schematic depicted in *Figure 1A* [GFP  
261 reporter gene under the regulation of a constitutive spleen focus-forming virus {SFFV}  
262 promoter]). In this context, the use of the tNGFR reporter is advantageous since it enables tracking  
263 and enrichment of the corrected cells and has been approved for clinical applications<sup>51</sup>. Our *KI-*  
264 *KO* approach mimics the correction in recessive SCID patient cells where a single functional allele  
265 is enough to confer the host with a normal immune system. The *KI* correction donor DNA  
266 contained complete *RAG2* cDNA with silent mutations added to diverge the cDNA sequence from  
267 that of endogenous while maintaining codon usage. The resulting diverged cDNA produces the  
268 correct protein sequence, while the reduced similarity to the genomic sequence precludes the

269 cDNA sequence from being re-cut by residual Cas9 or from serving as a potential homology arm  
270 causing premature cessation of HDR.<sup>52</sup> These *KI-KO* cells, double-positive for GFP and tNGFR,  
271 simulate the genotype and therapeutic outcome of *RAG2*-SCID single-allelic correction gene-  
272 editing therapy and were analyzed relative to our disease modeled biallelic *RAG2* KO cells.

273 *RAG2 KI-KO* CD34<sup>+</sup> HSPCs were sorted for double-positive tNGFR<sup>+</sup>/GFP<sup>+</sup> expression (HDR  
274 values in Figure S5A) and sorted cells were subjected to IVTD. To validate *RAG2* biallelic editing  
275 efficiency, targeted alleles were analyzed by ddPCR and found to be positive (Figure S5B).  
276 Additionally, quantitative real-time PCR (qRT-PCR) analysis revealed that the endogenous gene  
277 expression of *RAG2* was markedly reduced (Figure S5C) while robust diverged cDNA expression  
278 was found exclusively in the engineered cells (Figure S5D). Importantly, the expression of the  
279 diverged *RAG2* cDNA indeed facilitated T-cell development highlighted by the successful  
280 differentiation of *RAG2 KI-KO* edited cells into CD3<sup>+</sup> T cells relative to *RAG2* KO cells on day  
281 28 (*RAG2 KI-KO*: 2.7%; *RAG2* KO: 0.03%) (Figure 3B-C, Figure S5E-F).

282 Deep-sequencing analysis of TRG V(D)J recombination on days 14 and 28 revealed a diverse TRG  
283 V(D)J rearrangement repertoire in the *RAG2 KI-KO* population following robust expression of the  
284 *RAG2* diverged cDNA (Figure 4A). Moreover, calculation of Shannon and Simpson diversity  
285 indices revealed that there were no significant differences between the TRG clonotype diversity  
286 richness of *Mock*, *CCR5* KO, and *RAG2 KI-KO* populations (Figure 4B). Lastly, the frequency  
287 distribution of complementarity determining region 3 (CDR3) lengths was comparable to that of  
288 the control groups, indicating production of a diverse TCR repertoire (Figure S6). The CDR3  
289 region is responsible for recognizing processed antigen peptides and the length and sequence of  
290 the CDR3 varies by T-cell clone. Thus, the sequence of CDR3 determines the structure and  
291 specificity of the TCR, where a unique CDR3 sequence represents a specific T-cell clonotype.

292 Sequencing of the CDR3 region can, therefore, be used as a measurement of TCR diversity.<sup>53</sup>  
293 Together, these data indicate that *KI* of the correction diverged cDNA promotes differentiation  
294 into CD3<sup>+</sup> T cells and promotes the development of a highly diverse TRG repertoire.

### 295 ***RAG2* functional gene correction in *RAG2*-SCID-patient-derived CD34<sup>+</sup> HSPCs**

296 After determining that integration and expression of our correction donor were effective in  
297 facilitating T-cell development, we obtained CD34<sup>+</sup> HSPCs from the cord blood (CB) of a *RAG2*-  
298 SCID patient to actuate *in-vitro* functional gene correction. This patient presented with a clinical  
299 SCID phenotype (Omenn phenotype) and had compound heterozygous missense mutations  
300 (G95V+E480X) in the *RAG2* gene.<sup>54</sup> In compound heterozygotes, each allele of the gene has a  
301 different genetic mutation. In such cases, our approach is uniquely advantageous since we integrate  
302 the complete *RAG2* cDNA including the endogenous 3' UTR region at the initiation codon of the  
303 endogenous *RAG2* locus, thus resolving all possible mutations in the open reading frame while  
304 preserving the endogenous regulation and gene expression with a single rAAV6 donor.

305 Consequently, we aimed to target the *RAG2*-SCID CD34<sup>+</sup> HSPCs with *RAG2* diverged cDNA  
306 (schematic depicted in *Figure 3A*) using a rAAV6 MOI of 12,500 viral genomes (VG) per cell.  
307 Notably, however, we observed that when HD-derived CD34<sup>+</sup> HSPCs were treated with the *RAG2*  
308 correction donor at 12,500 VG/cell and subjected to the IVTD system, cellular yield was  
309 substantially reduced compared to samples that were not exposed to the rAAV6 vectors (*Figure*  
310 *S7A*). While the rAAV6 particles were found to be significantly diluted over the course of the  
311 IVTD process, they were still present by days 28 and 42 (*Figure S7B*) leading to increased cell  
312 death and/or reduced proliferation in the rAAV-treated populations, both hallmarks of prolonged  
313 rAAV-induced toxicity. Moreover, although two days post-electroporation (day 0) effective HDR

314 was observed in these cells via both flow cytometry and ddPCR (Figure S7C), we saw a decrease  
315 in targeted allele frequency via both methods over the 42 days of IVTD (Figure S7D-E). Therefore,  
316 to reduce the potential for similar results in the patient samples, cell sorting was used to enrich for  
317 corrected CD34<sup>+</sup> HSPCs using the tNGFR marker in two samples of RAG2-SCID (one treated at  
318 a MOI of 12,500 VG/cell and one at 6,250 VG/cell) (Figure S7F). We then subjected the sorted  
319 cells to the IVTD system, thus minimizing the risk of positive selection of unedited cells in the  
320 IVTD system. In parallel, HD-derived *Mock* CD34<sup>+</sup> HSPCs, untreated RAG2-SCID CD34<sup>+</sup>  
321 HSPCs, and unsorted RAG2-SCID corrected CD34<sup>+</sup> HSPCs (MOI of 12,500 VG/cell) were  
322 cultured in the IVTD system. For the sorted cells, ddPCR was performed to determine the extent  
323 of RAG2 cDNA genomic integration which was observed to be ~50% of all targeted alleles for  
324 both MOIs (Figure S7G). Following 28 days in the IVTD system, the RAG2-SCID corrected cells  
325 developed into CD3<sup>+</sup> cells, in all three corrective populations, compared to RAG2-SCID cells that  
326 showed impaired progression towards CD3 expression (12,500 VG/cell RAG2-SCID unsorted:  
327 2.7%; 12,500 VG/cell RAG2-SCID sorted: 6.0%; 6,250 VG/cell RAG2-SCID sorted: 6.2%; RAG2-  
328 SCID: 0.2%) (Figure 5). These data were comparable with CD3-expression levels of *Mock* cells  
329 (average of 5%) after 28 days in the IVTD system (Figure 5 and S7H). The percentage of CD3<sup>+</sup>  
330 cells in the population continued to rise by day 42 in the sorted populations similar to the *Mock*  
331 sample (Figure 5 and S7H). Additionally, an increase in cell death in the rAAV-treated populations  
332 was observed via cell viability staining, a hallmark of prolonged rAAV-induced toxicity (Figure  
333 S7I).

334 Deep sequencing of the TRG repertoire revealed that each of the two sorted populations developed  
335 a diverse TRG repertoire, highlighted throughout the IVTD timeline by treemap, CDR3 length,  
336 and Shannon and Simpson diversity indices (Figure 6A-B and Figure S8). We could not, however,

337 evaluate the repertoire of the unsorted *RAG2*-SCID correction cells at day 42 since only a very  
338 small number of CD3<sup>+</sup> cells survived until this time point (Figure 5). The richness of the observed  
339 TRG repertoires was comparable to that of the untreated *Mock* populations in the IVTD system  
340 (Figure 6B). To further examine the rearrangement capability, copies of T-cell receptor excision  
341 circles (TRECs) were quantified. TRECs, are a DNA marker that represents the excision of the  
342 delta-coding segments out of the T-cell receptor alpha (TRA) locus, allowing the TRA  
343 recombination to occur.<sup>55</sup> According to newborn screening data for SCID, TREC copies are  
344 completely undetectable in *RAG2*-SCID samples.<sup>4</sup> In our samples, TRECs were detected only in  
345 the sorted *RAG2*-SCID correction samples at day 28 and 42 of differentiation, with a higher copy  
346 number in the 6,250 *RAG2*-SCID corrected cells (Table 1). In summary, building off of our success  
347 with our correction donor in the *KI-KO* correction simulation approach, we were able to utilize the  
348 same donor to correct *RAG2*-SCID-patient-derived CD34<sup>+</sup> HSPCs *in vitro*, producing CD3<sup>+</sup> T cells  
349 with diverse TRG repertoires.

## 350 Discussion

351 Disease modeling is a fundamental part of understanding the mechanisms underlying the  
352 expression and regulation of the affected genes and due to their central roles in the T-cell  
353 development process, we chose to focus on the *RAG2*, *DCLRE1C*, and *IL7RA* genes. Patient-  
354 derived samples represent a natural system to study these mechanisms and their influence on the  
355 various cell processes, however, in diseases such as SCID, obtaining a sufficient quantity of CD34<sup>+</sup>  
356 HSPCs from young patients for scientific studies is not a viable option. In place, some researchers  
357 have generated iPSCs derived from dermal fibroblasts or skin keratinocytes of SCID patients in  
358 order to build disease models and to study the cells' differentiation potential.<sup>56-59</sup> This option has  
359 been widely accepted, however, iPSCs lack the authenticity of unadulterated CD34<sup>+</sup> HSPCs. We

360 present a novel approach to address this problem by modeling different recessive forms of SCID  
361 through biallelic CRISPR-Cas9/rAAV6-mediated gene *KO* in easily-attainable, abundant,  
362 biologically-authentic, HD-derived CD34<sup>+</sup> HSPCs. This strategy is made possible by multiplexing  
363 HDR using distinct reporter genes and sorting via FACS to enrich for complete biallelic *KO* cells.  
364 While in this work average biallelic HDR ranged from 1.7-4.6% (depending on the locus), we  
365 believe that enhancing HDR by reducing toxic rAAV6-induced DDR and/or inhibiting the NHEJ  
366 repair pathway, among other techniques, we can further improve our method.<sup>60,61</sup>

367 We tracked the biallelic *KO* cells in a stromal cell-free IVTD system to better understand the SCID  
368 phenotype to subsequently use as confirmation for the success of our proof-of-concept correction  
369 phenotype. The readout of our system is multi-faceted, allowing for immunophenotyping via flow  
370 cytometry to track T-cell differentiation and NGS for TCR repertoire analysis. We believe that  
371 using this system for disease modeling via CRISPR-Cas9 editing has the potential to rapidly  
372 accelerate research on suspected disease-causing genes. These disease models can then be  
373 phenotypically and functionally validated in various differentiation platforms paving the way for  
374 new potential gene therapies.

375 One of the challenges when modeling SCID disease is effectively inducing a reproducible T-cell  
376 differentiation phenotype.<sup>62</sup> A recent study by Pavel-Dinu *et al.* presented an approach for *IL2RG*  
377 gene correction on male HD-derived CD34<sup>+</sup> HSPCs and SCID-X1 patient samples cultured in the  
378 *in-vitro* OP9 T-cell differentiation system. A major drawback of the OP9 system is the difficulty  
379 of efficiently differentiating PB CD34<sup>+</sup> HSPCs while obtaining a consistent differentiation  
380 pattern.<sup>62-64</sup> Hence, Pavel-Dinu *et al.* addressed this problem by assessing the differentiation  
381 pattern of *IL2RG* HDR-corrected CD34<sup>+</sup> HSPCs after transplantation to NSG mice. Through  
382 enrichment of edited cells via sorting and subsequent use of a stromal cell-free IVTD system we

383 have overcome the variability challenges encountered in other T-cell differentiation studies. Thus,  
384 we established a sustainable, versatile, and reproducible system for evaluating gene-correction  
385 efficiency and studying the mechanisms of recessive forms of SCID that allows for easy cell  
386 tracking, immunophenotyping, and V(D)J recombination analyses.

387 With the use of the IVTD system, we showed the successful differentiation of HD-derived CD34<sup>+</sup>  
388 HSPCs to CD7<sup>+</sup>CD5<sup>+</sup> cells and eventually to CD4, CD8, and CD3-expressing T cells, with diverse  
389 TRG repertoires. *RAG2* biallelic KO and *DCLRE1C* biallelic KO CD34<sup>+</sup> HSPCs developed into  
390 CD7<sup>+</sup>CD5<sup>+</sup> cells, however, did not develop further to express CD3 and did not exhibit TRG gene  
391 rearrangement. Previously, Bifsha *et al.* and Bosticardo *et al.* assessed the T-cell differentiation  
392 outcome of SCID-patient-derived PB CD34<sup>+</sup> HSPCs via the OP9 IVTD system and the artificial  
393 thymic organoids (ATO) system, respectively.<sup>62,65</sup> In their work, the *RAG2* patient cells displayed  
394 a developmental failure at the same T-cell differentiation stage (CD3-expressing stage) as we  
395 observed in our disease models as well as in the SCID-patient-derived PB CD34<sup>+</sup> HSPC samples.  
396 Curiously, clinical analysis of *RAG2*-SCID patients c.G104T and p.G95V+E480X showed  
397 expression of CD3 (Table S1 and S2) despite the lack of differentiation of the same patients'  
398 CD34<sup>+</sup> HSPCs into CD3<sup>+</sup> cells in the IVTD system. Although patients with SCID typically present  
399 profoundly reduced total T cell counts, patients can sometimes display the presence of self-reactive  
400 cells and trans-placentally acquired maternal T cells.<sup>66</sup> This could explain the discrepancy between  
401 clinical blood analysis and the output of our IVTD method. Taken together, modeling recessive  
402 forms of SCID via CRISPR-Cas9/rAAV6 gene editing coupled with the use of the highly  
403 reproducible IVTD system can effectively limit the requirement for large quantities of scarce  
404 patient-derived samples.

405 As mentioned, we chose to focus on the *RAG2*, *DCLRE1C*, and *IL7RA* genes which combined are  
406 responsible for ~21% of all SCID cases in the United States of America, while *DCLRE1C* and  
407 *IL7RA* mutations alone were responsible for 59.3% of all SCID cases in Israel.<sup>3,4,7</sup> Even when a  
408 HLA-matched donor is found and allogeneic HSCT is conducted, patient outcomes for *RAG*-  
409 SCIDs are significantly worse than for T-B+NK- SCIDs such as SCID-X1.<sup>67,68</sup> *RAG*-SCIDs  
410 present a T-/B-/NK+ phenotype and the presence of NK cells has been shown to mediate graft  
411 rejection in murine SCID models as well as in human observational studies.<sup>69</sup> Thus, development  
412 of other treatment options for these SCIDs such as autologous gene therapy is critical to eliminate  
413 the need for finding an HLA-matched donor and to limit the risk of graft rejection.

414 Although great strides have been made in the past few decades, gene therapy using viral vectors  
415 in its current form ( $\gamma$ RV or LV) could be hazardous for highly controlled and regulated genes such  
416 as *RAG1* and *RAG2* due to the constitutive expression of the transgene. In these cases, this can  
417 result in genomic instability, and in some cases leukemia, as a result of expression outside of the  
418 precise developmental window.<sup>70-72</sup> A recent study by Miyazaki *et al.* demonstrated that the  
419 mechanism for developmental regulation of *RAG1/2* gene expression is via cis-elements  
420 surrounding the *RAG1/2* coding regions which control the spatial genomic organization inside the  
421 locus.<sup>73</sup> Additionally, Rommel *et al.* found that aberrantly functioning *RAG1/2* promotes  
422 lymphocyte malignancy through the formation of translocations and/or deletions in cancer-causing  
423 genes.<sup>74</sup> To address this, we aimed to establish a gene-editing method that addresses gene  
424 regulation and integration specificity. In our study, the *RAG2* sgRNA used for gene correction was  
425 designed to induce a specific DSB several base pairs downstream to the gene's ATG start codon  
426 and the diverged cDNA delivered by the rAAV6 included the gene's endogenous 3' UTR. In  
427 contrast to the strategy employed in Pavel-Dinu *et al.*, our method allowed for the subsequent

428 expression of the transgene to rely on the conserved endogenous 5' and 3' transcriptional and  
429 translational regulatory elements.<sup>75</sup> To ensure the safety of our gene-editing strategy the *RAG2*  
430 sgRNA's off-target potential was previously thoroughly examined, ensuring that it edits only a  
431 small number of off-target sites with low editing frequency.<sup>76,77</sup> Our approach highlights the  
432 importance of safeguarding the regulatory elements that are located outside of the coding region  
433 and the importance of inducing precise integration of transgenic elements.

434 After establishing a novel disease model, we proceeded to evaluate a proof-of-concept CRISPR-  
435 Cas9/rAAV6 gene-correction strategy through our *KI-KO* approach in HD-derived CD34<sup>+</sup> HSPCs.  
436 Since *RAG2-SCID* is an autosomal recessive disorder, correction of only one allele is required to  
437 have the patient develop a functional immune system, hence our use of a single-allelic *KI* while  
438 the other allele is *KO* (mimicking a mutated allele). While theoretically one could employ a *KI*  
439 strategy and rely on Cas9-induced INDELS for the *KO* of the other allele, our *KI-KO* method is  
440 more definitive for two reasons. 1) The INDEL efficiencies for sgRNAs although highly-efficient,  
441 are not 100%. Thus, even if it is a small amount, there will be cells that will not have a *KI-KO*  
442 genotype. 2) Our approach, although applied here for *RAG2* alone is an approach that can be  
443 applied universally to any monogenic disorder. In each case, the gene-specific sgRNA would have  
444 its own unique INDEL signature, not always leading to gene *KO*. Thus, a uniform HDR-based  
445 biallelic *KI-KO* approach is beneficial. Our correction simulation using *RAG2* diverged cDNA  
446 expression led to successful T-cell differentiation highlighted by successful TRG gene  
447 rearrangement and expression of T-cell markers, CD4, CD8, and CD3. This allowed us to test our  
448 correction donor on HD-derived CD34<sup>+</sup> HSPCs before utilizing any precious patient-derived  
449 samples. With the confidence in our system, we then actuated the first-of-its-kind, successful, *in-*

450 *vitro* correction of RAG2-SCID-patient-derived CD34<sup>+</sup> HSPCs, which, post-correction, produced  
451 CD3-expressing T cells with a diverse TRG repertoire.

452 Based on previously studied cases of “naturally-occurring gene therapy” where a revertant  
453 mutation led to the unexpected development of T lymphocytes and diverse TCR repertoires in  
454 SCID patient, it is assumed that individual corrected cells are capable of at-least partially  
455 correcting the SCID phenotype. In these cases, it is estimated that a single cell with the corrective  
456 revertant mutation was able to undergo ~11 divisions before undergoing TCR gene arrangements,  
457 thus giving way to ~1,000 unique TCR sequences.<sup>78-81</sup> These cases highlighted the fact that even  
458 a small number of “corrected” cells can generate a fully diversified TCR repertoire enough to  
459 reconstitute the immune system. Additionally, 5-10% donor chimerism is considered to be the  
460 threshold for successful clinical improvement for SCID patients post-allogenic HSCT. Dvorak *et*  
461 *al.* showed that donor chimerism as low as 3% was sufficient for T- and B-cell recovery in SCID  
462 patients in contrast to greater than 20% for diseases such as thalassemia or sickle cell anemia.<sup>82</sup>

463 While rAAV6 is commonly used to deliver the donor DNA in genome-editing experiments, our  
464 group has shown in Allen *et al.* that rAAV6 vectors can trigger a potentially toxic DDR after  
465 entering cells proportional to the MOI used.<sup>42</sup> In order for CRISPR/rAAV6 treatments to be  
466 implemented as a clinical therapy for the purpose of gene correction, reduction of the rAAV6  
467 toxicity is required. We demonstrated that lowering the MOI (from 12,500 to 6,250 VG/cell)  
468 maintains HDR of  $\geq 17\%$  and allows for potential alleviation of rAAV6-induced genotoxicity as  
469 noted by higher levels of TREC copy numbers as well as higher CD3 expression in the 6,250  
470 VG/cell sample (Figure 5 and Table 1). Additionally, we noted a difference between the sorted  
471 and unsorted 12,500 VG/cell populations on day 28 and day 42 in the frequency of CD3<sup>+</sup> cells.  
472 We hypothesize that this is due to lower input of corrected cells to our IVTD system as well as

473 competition between the corrected and uncorrected cells in our IVTD system in the unsorted  
474 sample. Due to these challenges, we observed a drop off in CD3 expression in the unsorted sample  
475 while the CD3-expressing population in the comparable sorted sample expanded from 6% on day  
476 28 to 19% on day 42. Based on this new understanding of the effects of MOI and cell enrichment,  
477 we propose the following possible ways to counter this reduction in efficacy: 1) Improving HDR  
478 efficiency by inhibiting the NHEJ repair pathway via molecules such as i53 and/or DNA-PK  
479 inhibitors; 2) Transiently suppressing p53 to rescue the toxic DDR; and/or 3) Enrichment of the  
480 corrected cell population via cell sorting.<sup>60,61</sup> Additionally, we are currently working towards using  
481 good manufacturing practices (GMP) grade rAAV6 preparations, free of potential toxic impurities.  
482 This will enable us to expand our research to animal models and eventually to the clinic. Although  
483 follow-up studies are ongoing to improve HDR efficiencies, thus increasing the feasibility of  
484 achieving high donor chimerism frequencies without cell enrichment, our enrichment strategy  
485 enables ~100% HDR input frequency after cell sorting which together with the relatively low  
486 threshold for requisite donor chimerism in SCID patients, provides a valuable proof-of-concept  
487 correction methodology.

488 In summary, we present a disease model for SCID and proof-of-concept gene therapy using a  
489 combination of CRISPR-Cas9, rAAV6 donors, a reproducible cell-free IVTD system, and  
490 abundant HD-derived CD34<sup>+</sup> HSPCs. This system allows for circumventing the difficulty of  
491 obtaining large amounts of patient samples while providing a valuable tool that will allow  
492 researchers to find the optimal gene-editing configurations (i.e. engineered nuclease and donor  
493 DNA) for SCID and other additional recessive blood disorders. Lastly, since we use authentic  
494 CD34<sup>+</sup> HSPCs as opposed to iPSCs, cell lines, or cells that no longer maintain their stemness, we

495 believe that the feasibility of translating our gene correction strategy to the clinic will be simpler  
496 highlighted by our successful correction of *RAG2-SCID*-patient-derived CD34<sup>+</sup> HSPCs.

## 497 **Materials and Methods**

### 498 **CD34<sup>+</sup> HSPCs Purification**

499 CD34<sup>+</sup> HSPCs were isolated from CB samples collected at Sheba Medical Center CB Bank under  
500 Institutional Review Board - approved protocols to obtain CB units for research purposes.  
501 Informed consent was signed indicating that cord blood specimens that are not suitable for banking  
502 will be used for research. Mononuclear cells (MNCs) were separated from fresh CB samples by  
503 Lymphoprep™ density gradient medium (STEMCELL Technologies Inc.). Frozen CB samples  
504 were thawed and treated with 5,000 U/ml of DNase I (Worthington). Using the CD34<sup>+</sup> Microbead  
505 Kit Ultrapure (Miltenyi Biotec), CD34<sup>+</sup> HSPCs were purified from the MNCs by CD34 labeling  
506 according to the manufacturer's protocol. Enriched CD34<sup>+</sup> HSPCs were stained with APC anti-  
507 human CD34 antibodies (clone 581, Biolegend, San Jose, CA, USA), and sample purity was  
508 assessed on an Accuri C6 flow cytometer (BD Biosciences, San Jose, CA, USA). Cells were  
509 cryopreserved in CryoStor® CS10 medium (STEMCELL Technologies Inc.) or were cultured for  
510 48 hours at a density of  $2.5 \times 10^5$  cells/ml in StemSpan SFEM II (STEMCELL Technologies Inc.)  
511 supplemented with Stem Cell Factor (SCF) (100 ng/ml), Thrombopoietin (TPO) (100 ng/ml), Fms-  
512 like tyrosine kinase 3 ligand (Flt3-Ligand) (100 ng/ml), Interleukin 6 (IL-6) (100 ng/ml),  
513 StemRegenin 1 (SR1) (0.75 mM), UM171 (35 nM) (STEMCELL Technologies Inc.), and 1%  
514 Penicillin/Streptomycin (Biological Industries Israel Beit Haemek LTD). Cells were cultured at  
515 37°C, 5% CO<sub>2</sub>, and 5% O<sub>2</sub>. The PB samples were obtained at Sheba Medical Center under  
516 Institutional Review Board. Informed consent was signed to ensure that specimens will be used

517 only for research purposes. CD34<sup>+</sup> HSPCs from PB *RAG1* and *RAG2* SCID patients, and from  
518 healthy donors were isolated by negative selection using RossetaSep<sup>®</sup> (STEMCELL Technologies  
519 Inc.). Cells from the fractionated plasma layer were enriched by Lymphoprep<sup>™</sup> density gradient  
520 medium (STEMCELL Technologies Inc.) and subsequently stained and sorted for APC human  
521 CD34<sup>+</sup> (clone 581, Biolegend) and FITC human CD45<sup>low</sup> (clone HI30, BD Pharmingen)  
522 expression by Aria III cell sorter (BD Biosciences). Post-sort, cells were stained with PE/Cy7-  
523 CD7 (clone:CD7-6B7, BioLegend) and BV421-CD5 (clone: UCHT2, BioLegend) and were  
524 analyzed by LSRFortessa<sup>™</sup> cell analyzer (BD Biosciences).

### 525 **rAAV6 Donor DNA Template Design**

526 All rAAV6 vector plasmids were cloned using NEBuilder<sup>®</sup> HiFi DNA Assembly Master Mix (cat  
527 # E2621L, New England Biolabs (NEB) Inc.) into the pAAV-MCS plasmid (Agilent Technologies  
528 containing inverted terminal repeats (ITRs). Each rAAV6 disruption donor contains a different  
529 reporter gene (GFP, tNGFR, or tdTomato) under the control of a SFFV promoter and followed by  
530 a BGH polyA sequence. The *RAG2* correction rAAV6 donor was designed and contains diverged  
531 *RAG2* cDNA followed by the *RAG2* 3'UTR and a reporter gene (tNGFR) controlled by a PGK  
532 promoter and BGH polyA sequence. Each donor DNA was designed with 400bp left and right  
533 homology arms flanking the sgRNA cut site. The rAAV6 vectors were produced by Vigene  
534 Biosciences in large-scale rAAV6 packaging. See Table S5 for the DNA donor sequences.

### 535 **CRISPR-Cas9 Genome Targeting and Biallelic Integration**

536 *RAG2* and *CCR5* modified sgRNAs, previously described, were synthesized by TriLink  
537 BioTechnologies.<sup>37,76</sup> *IL7RA* and *DCLRE1C* modified sgRNAs were synthesized by Integrated  
538 DNA Technologies (IDT, Coralville, IA). The 20 bp sgRNA genomic target sequences were as

539 follows: *RAG2*: 5'-UGAGAAGCCUGGCUGAAUUA-3', *CCR5*: 5'-  
540 GCAGCAUAGUGAGCCCAGAAG-3', *IL7RA*: 5'-ACAAUUCUAGGUACAACUUU-3', and  
541 *DCLRE1C*: 5'-GCGCUAUGAGUUCUUUCGAG-3'. 260 pmol of sgRNA was complexed pre-  
542 electroporation with 104 pmol of Alt-R Cas9 protein (IDT, Coralville, IA) forming an RNP  
543 complex, at a 1:2.5 molar ratio (Cas9:sgRNA). Electroporation of CD34<sup>+</sup> HSPCs was performed  
544 with P3 nucleofection solution (Lonza, Basel, Switzerland) in the Lonza Nucleofector 4D  
545 (program DZ-100). INDEL quantification was performed via the tracking of INDELs by  
546 decomposition (TIDE) analysis platform (available at <https://tide.nki.nl/>). Electroporated CD34<sup>+</sup>  
547 HSPCs were plated at 4 x 10<sup>5</sup> cells/ml and transduction of disruption *RAG2* donors was performed  
548 at a MOI of 6,250 VG/cell for each donor. The MOI for the *RAG2* correction rAAV6 in HD-  
549 derived CD34<sup>+</sup> HSPCs was 12,500 VG/cell, and for *RAG2*-SCID CD34<sup>+</sup> HSPCs the MOI was  
550 6,250 or 12,500 VG/cell. For *IL7RA* rAAV6 disruption donors, GFP and tdTomato, MOIs were  
551 12,500 VG/cell and 25,000 VG/cell, respectively. For *DCLRE1C* rAAV6 disruption donors, GFP  
552 and tdTomato, the MOI was 12,500 VG/cell for each donor. rAAV6 donors were added to the  
553 plated cells, within 15 minutes of electroporation. After 24 hours, fresh CD34<sup>+</sup> medium was added  
554 to form a final concentration of 2.5 x 10<sup>5</sup> cells/ml. 48 hours post-electroporation, cells were  
555 collected and prepared for the biallelic enrichment by the Aria III cell sorter (BD Biosciences).  
556 Cells were stained with PE human CD34 (clone: 561, BioLegend) antibodies, and when rAAV6  
557 tNGFR is transduced APC-tNGFR (clone: ME20.4, BioLegend) staining is performed as well.

### 558 **INDEL Frequency Quantification via NGS**

559 On-target NGS for the *RAG2* sgRNA was conducted by our group and reported previously and the  
560 FASTQ files were downloaded for additional analysis using the CRISPECTOR software tool from  
561 the sequence read archive (SRA) under accession number PRJNA628100.<sup>76,83</sup>

**562 Digital Droplet PCR™**

563 The quantification of genomic integration was performed by Digital Droplet PCR™ (ddPCR™,  
564 Bio-Rad, Hercules, CA, USA). Genomic DNA was extracted from sorted populations cultured in  
565 CD34<sup>+</sup> medium and IVTD using GeneJET Genomic DNA Purification Kit (Thermo Fisher  
566 Scientific, USA). Each ddPCR reaction mix contains a HEX reference assay detecting copy  
567 number input of the *CCRL2* gene to quantify the chromosome 3 input. Separate assays with a set  
568 of target-specific primers and a FAM-labeled probe (500 nM and 250 nM, respectively) for each  
569 gene were used to detect the locus specific donor integration. The reaction was carried as follows:  
570 10 µl ddPCR Supermix for Probes No dUTP (Bio-Rad), 1 µl of each PrimeTime® Standard qPCR  
571 Assay (IDT, Coralville, IA), µl of a restriction enzyme mix [1/2 EcoRI-HF® (NEB #R3101, 2/5  
572 Nuclease-free water, 1/10 CutSmart Buffer 10X (NEB)], 20 ng genomic template DNA, and  
573 supplemented to a total of 20 µl with Nuclease-free water. Droplet samples were prepared  
574 according to manufacturer's protocol (Bio-Rad) and 40 µl of the droplets were conveyed to a 96-  
575 well plate and amplified in a Bio-Rad PCR thermocycler with the following PCR conditions: 1  
576 cycle at 95°C for 10 minutes, followed by 40 cycles at 95°C for 30 seconds and then 55°C for 3  
577 minutes, followed by 1 cycle at 98°C for 10 minutes at a ramp rate of 2.2°C/s. After the PCR, the  
578 96-well plate was loaded in the QX200 droplet reader (Bio-Rad). The droplets from each well were  
579 analyzed and the concentration of copies/µl of the site-specific donor integration (FAM) and wild-  
580 type *CCRL2* (HEX) alleles were calculated using the QuantaSoft analysis software (Bio-Rad).  
581 Primers and probes sequences are presented in Table S3.

**582 Estimation of mRNA Levels in Differentiated T Cells**

583 RNA was extracted using Direct-zol™ RNA Miniprep Plus (Zymo Research, cat #R2073) from  
584 differentiated T cells obtained on days 14 and 28 of IVTD. cDNA was prepared from 50-150 ng  
585 RNA, using Oligo d(T)23 VN- S1327S (NEB), dNTPs 10mM, and M-MuLV Reverse  
586 Transcriptase (cat# M0253S, NEB). qRT-PCR reactions were done using TaqMan® Fast  
587 Advanced Master Mix (cat# AB-4444557, Thermo Fisher Scientific) and carried out on  
588 StepOnePlus™ Real-Time PCR System (cat# 4376600, Thermo Fisher Scientific). PCR  
589 conditions were as follows: uracil-N-glycosylase gene (UNG) incubation was 2 minutes at 50°C,  
590 polymerase activation was 20 seconds at 95°C, followed by 40 cycles of 1 second at 95°C and 20  
591 seconds at 60°C. Primers and probes sequences are presented in Table S4.

#### 592 ***in-vitro* T-cell Differentiation System**

593 Using StemSpan™ T Cell Generation Kit (STEMCELL Technologies, Inc.), CD34<sup>+</sup> HSPCs were  
594 cultured in StemSpan™ SFEM II containing Lymphoid Progenitor Expansion Supplement on  
595 plates coated with Lymphoid Differentiation Coating Material for 14 days. Subsequently, cells  
596 were harvested and re-seeded on coated plates with StemSpan™ T Cell Progenitor Maturation  
597 Supplement for an additional 14 days. PB and CB CD34<sup>+</sup> HSPCs experiments, were re-seeded on  
598 coated plates with StemSpan™ T Cell Progenitor Maturation Supplement at day 28 of culturing  
599 and harvested at day 42 of differentiation. Flow cytometry analysis was conducted at each time  
600 point of differentiation using the LSRFortessa™ cell analyzer (BD Biosciences). On day 14,  
601 collected cells were stained with PE/Cy7-CD7 (clone:CD7-6B7, BioLegend), BV421-CD5 (clone:  
602 UCHT2, BioLegend), and CD1a-PE (clone: BL6, Beckman Coulter, USA) or CD1a-APC (clone:  
603 BL6, Beckman Coulter, USA) antibodies. On days 28 and 42, collected cells were stained with  
604 PE/Cy7-CD4 (clone: RPA-T4, BioLegend), APC-r700-CD8a (clone: RPA-T8, BD Horizon™),  
605 and BV421-CD3 (clone: UCHT1, BioLegend) antibodies. BD Horizon™ Fixable Viability Stain

606 510 was performed on all the collected cells at each time point. APC-NGFR (clone: ME20.4,  
607 BioLegend) staining was conducted on all tNGFR rAAV6 integrated cells. For evaluating the  
608 background staining, fluorescence minus one (FMO) + isotype control antibody staining was  
609 performed using the following isotypes: PE/Cy7 Mouse IgG2a  $\kappa$  (cat # 400232, BioLegend), BV-  
610 421 Mouse IgG1  $\kappa$  (cat # 400158, BioLegend), PE Mouse IgG1  $\kappa$  (cat # 400112, BioLegend),  
611 PE/Cy7 Mouse IgG1  $\kappa$  (cat # 400126, BioLegend), APC-R700 Mouse IgG1  $\kappa$  (cat #564974, BD  
612 Horizon™), and APC Mouse IgG1  $\kappa$  (cat # 400122, BioLegend).

### 613 **Identification of TRG Gene Rearrangements**

614 gDNA from differentiated T cells and CD34<sup>+</sup> HSPCs was extracted by the GeneJET Genomic  
615 DNA Purification Kit (Thermo Fisher Scientific). TRG rearrangement was assessed by PCR  
616 amplification of 12 possible CDR3 clones, using combinations of 4 primers for V $\gamma$  and 3 primers  
617 for J $\gamma$  regions in each reaction (IdentiClone™ TCRG Gene Clonality Assay, Invivoscribe, Inc.).  
618 TRG clonality was ran and analyzed on 2% agarose gel. For deep sequencing of the TRG  
619 repertoire, the TRG rearranged genomic products were amplified using a single multiplex master  
620 mix LymphoTrack® TRG assay (Invivoscribe, Inc.). PCR amplicons were purified and sequenced  
621 using the Miseq V2 (500 cycles) kit, 250-bp paired-end reads (Illumina, San Diego, CA). FASTQ  
622 files were analyzed by LymphoTrack Software (Invivoscribe, Inc.). LymphoTrack Software  
623 unique sequences generated data of each sample that was further analyzed by the IMGT® software,  
624 the international ImMunoGeneTics information system® (HighV-QUEST, <http://www.imgt.org>).  
625 The analysis of the incidence of productive and unproductive TRG rearrangements sequences were  
626 performed amidst the total sequences and presented visually by TreeMap 2019.3.2 software  
627 (Macrofocus GmbH). Unique sequences and CDR3 length analysis were obtained from the total  
628 productive sequences. The Shannon's H and Simpson's D diversity indices were calculated by

629 PAST software.<sup>84</sup> The sequencing data were deposited to the Sequence Read Archive (SRA), under  
630 accession number: PRJNA838341.

### 631 **Quantification of TRECs**

632 TREC copy numbers were analyzed by qPCR, as previously described.<sup>85</sup> DNA samples were  
633 examined in triplicates, 100 ng for each replicate. qPCR reactions were carried out on  
634 StepOnePlus™ Sequence Detector System (Applied Biosystems). A standard curve was  
635 assembled by utilizing serial dilutions with  $10^3$ - $10^6$  copies of TREC plasmid. RNase P  
636 amplification (TaqMan assay, Applied Biosystems) was conducted for quality control of the DNA  
637 TREC amplification.

### 638 **Acknowledgments**

639 We would like to thank the members of the Somech and the Hendel Labs for reading the  
640 manuscript and providing practical advice. Additionally, we want to thank Dr. Rasmus O. Bak,  
641 and Dr. Andreas Reinisch for numerous important discussions and comments. Lastly, we would  
642 like to thank D. Russell for providing the pDGM6 plasmid. This work was supported by the  
643 European Research Council (ERC) under the European Union Horizon 2020 research and  
644 innovation program (grant number. 755758, A.H.), Israel Science Foundation (grant number.  
645 2031/19, A.H.), and Israel Precision Medicine Program (grant number. 3115/19, R.S., A.H., and  
646 Y.N.L). *Figure S3A* was created with BioRender.com.

### 647 **Author Contributions**

648 O.I., D.A., O.K., Y.Z., D.B., A.A., and A.L. designed and conducted the experiments, evaluated,  
649 and analyzed the data; O.I. and D.B. performed the bioinformatics analyses, with the help and

650 guidance of Y.N.L.; K.B., and A.N. provided cord blood samples and R.S. provided PB samples;  
651 K.B., Y.N.L., A.N., and R.S. critically reviewed the experiments and provided important advice;  
652 A.H. supervised and conceived the research and planned the experiments and the approaches;  
653 A.H., D.A., O.I., and Y.Z. wrote the manuscript, with contributions from all authors.

#### 654 **Declaration of Interests**

655 The authors declare that they have no known competing financial interests or personal  
656 relationships that could have appeared to influence the work reported in this paper.

#### 657 **Supplemental Information**

658 Supplemental data. Figures S1–S7; Tables S1-S4.

659 Table S5. rAAV6 donor DNA sequences.

#### 660 **Data Availability Statement**

661 The authors declare that all data supporting the findings of this study are available within the paper  
662 and its supplemental information files.

#### 663 **Key Words**

664 CRISPR-Cas9, rAAV6, HSPCs, genome editing, gene regulation, *RAG2*, SCID

#### 665 **References**

- 666 1. Barron, M.A., Makhija, M., Hagen, L.E., Pencharz, P., Grunebaum, E., and Roifman, C.M.  
667 (2011). Increased resting energy expenditure is associated with failure to thrive in infants  
668 with severe combined immunodeficiency. *J Pediatr* 159, 628-632 e621.  
669 10.1016/j.jpeds.2011.03.041.

- 670 2. Cirillo, E., Giardino, G., Gallo, V., D'Assante, R., Grasso, F., Romano, R., Di Lillo, C.,  
671 Galasso, G., and Pignata, C. (2015). Severe combined immunodeficiency--an update.  
672 *Annals of the New York Academy of Sciences* 1356, 90-106. 10.1111/nyas.12849.
- 673 3. Kwan, A., Abraham, R.S., Currier, R., Brower, A., Andruszewski, K., Abbott, J.K., Baker,  
674 M., Ballow, M., Bartoshesky, L.E., Bonilla, F.A., Brokopp, C., et al. (2014). Newborn  
675 screening for severe combined immunodeficiency in 11 screening programs in the United  
676 States. *JAMA* 312, 729-738. 10.1001/jama.2014.9132.
- 677 4. Rechavi, E., Lev, A., Simon, A.J., Stauber, T., Daas, S., Saraf-Levy, T., Broides, A.,  
678 Nahum, A., Marcus, N., Hanna, S., Stepensky, P., et al. (2017). First Year of Israeli  
679 Newborn Screening for Severe Combined Immunodeficiency-Clinical Achievements and  
680 Insights. *Front Immunol* 8, 1448. 10.3389/fimmu.2017.01448.
- 681 5. Kumrah, R., Vignesh, P., Patra, P., Singh, A., Anjani, G., Saini, P., Sharma, M., Kaur, A.,  
682 and Rawat, A. (2020). Genetics of severe combined immunodeficiency. *Genes Dis* 7, 52-  
683 61. 10.1016/j.gendis.2019.07.004.
- 684 6. Picard, C., Al-Herz, W., Bousfiha, A., Casanova, J.L., Chatila, T., Conley, M.E.,  
685 Cunningham-Rundles, C., Etzioni, A., Holland, S.M., Klein, C., Nonoyama, S., et al.  
686 (2015). Primary Immunodeficiency Diseases: an Update on the Classification from the  
687 International Union of Immunological Societies Expert Committee for Primary  
688 Immunodeficiency 2015. *J Clin Immunol* 35, 696-726. 10.1007/s10875-015-0201-1.
- 689 7. Lev, A., Sharir, I., Simon, A.J., Levy, S., Lee, Y.N., Frizinsky, S., Daas, S., Saraf-Levy, T.,  
690 Broides, A., Nahum, A., Hanna, S., et al. (2022). Lessons Learned from Five Years of  
691 Newborn Screening for Severe Combined Immunodeficiency (SCID) in Israel. *J Allergy*  
692 *Clin Immunol Pract*. 10.1016/j.jaip.2022.04.013.
- 693 8. Notarangelo, L.D., Kim, M.S., Walter, J.E., and Lee, Y.N. (2016). Human RAG mutations:  
694 biochemistry and clinical implications. *Nat Rev Immunol* 16, 234-246.  
695 10.1038/nri.2016.28.
- 696 9. Rooney, S., Sekiguchi, J., Zhu, C., Cheng, H.L., Manis, J., Whitlow, S., DeVido, J., Foy,  
697 D., Chaudhuri, J., Lombard, D., and Alt, F.W. (2002). Leaky Scid phenotype associated  
698 with defective V(D)J coding end processing in Artemis-deficient mice. *Molecular cell* 10,  
699 1379-1390. 10.1016/s1097-2765(02)00755-4.
- 700 10. Schatz, D.G., and Ji, Y. (2011). Recombination centres and the orchestration of V(D)J  
701 recombination. *Nat Rev Immunol* 11, 251-263. 10.1038/nri2941.
- 702 11. Kittipatarin, C., and Khaled, A.R. (2007). Interlinking interleukin-7. *Cytokine* 39, 75-83.  
703 10.1016/j.cyto.2007.07.183.
- 704 12. Gennery, A.R., Slatter, M.A., Grandin, L., Taupin, P., Cant, A.J., Veys, P., Amrolia, P.J.,  
705 Gaspar, H.B., Davies, E.G., Friedrich, W., Hoenig, M., et al. (2010). Transplantation of  
706 hematopoietic stem cells and long-term survival for primary immunodeficiencies in  
707 Europe: entering a new century, do we do better? *J Allergy Clin Immunol* 126, 602-610  
708 e601-611. 10.1016/j.jaci.2010.06.015.
- 709 13. Pai, S.Y., Logan, B.R., Griffith, L.M., Buckley, R.H., Parrott, R.E., Dvorak, C.C., Kapoor,  
710 N., Hanson, I.C., Filipovich, A.H., Jyonouchi, S., Sullivan, K.E., et al. (2014).  
711 Transplantation outcomes for severe combined immunodeficiency, 2000-2009. *N Engl J*  
712 *Med* 371, 434-446. 10.1056/NEJMoa1401177.
- 713 14. Schuetz, C., Neven, B., Dvorak, C.C., Leroy, S., Ege, M.J., Pannicke, U., Schwarz, K.,  
714 Schulz, A.S., Hoenig, M., Sparber-Sauer, M., Gatz, S.A., et al. (2014). SCID patients with  
715 ARTEMIS vs RAG deficiencies following HCT: increased risk of late toxicity in ARTEMIS-  
716 deficient SCID. *Blood* 123, 281-289. 10.1182/blood-2013-01-476432.
- 717 15. Cossu, F. (2010). Genetics of SCID. *Italian journal of pediatrics* 36, 76. 10.1186/1824-  
718 7288-36-76.
- 719 16. Cowan, M.J., and Gennery, A.R. (2015). Radiation-sensitive severe combined  
720 immunodeficiency: The arguments for and against conditioning before hematopoietic cell

- 721 transplantation--what to do? *J Allergy Clin Immunol* 136, 1178-1185.  
 722 10.1016/j.jaci.2015.04.027.
- 723 17. Cicalese, M.P., and Aiuti, A. (2015). Clinical applications of gene therapy for primary  
 724 immunodeficiencies. *Hum Gene Ther* 26, 210-219. 10.1089/hum.2015.047.
- 725 18. Booth, C., Gaspar, H.B., and Thrasher, A.J. (2016). Treating Immunodeficiency through  
 726 HSC Gene Therapy. *Trends Mol Med* 22, 317-327. 10.1016/j.molmed.2016.02.002.
- 727 19. Dever, D.P., Bak, R.O., Reinisch, A., Camarena, J., Washington, G., Nicolas, C.E., Pavel-  
 728 Dinu, M., Saxena, N., Wilkens, A.B., Mantri, S., Uchida, N., et al. (2016). CRISPR/Cas9  
 729 beta-globin gene targeting in human haematopoietic stem cells. *Nature* 539, 384-389.  
 730 10.1038/nature20134.
- 731 20. Naldini, L. (2011). Ex vivo gene transfer and correction for cell-based therapies. *Nat Rev*  
 732 *Genet* 12, 301-315. 10.1038/nrg2985.
- 733 21. De Ravin, S.S., Wu, X., Moir, S., Anaya-O'Brien, S., Kwatema, N., Littel, P., Theobald,  
 734 N., Choi, U., Su, L., Marquesen, M., Hilligoss, D., et al. (2016). Lentiviral hematopoietic  
 735 stem cell gene therapy for X-linked severe combined immunodeficiency. *Sci Transl Med*  
 736 8, 335ra357. 10.1126/scitranslmed.aad8856.
- 737 22. Marquez Loza, L.I., Yuen, E.C., and McCray, P.B., Jr. (2019). Lentiviral Vectors for the  
 738 Treatment and Prevention of Cystic Fibrosis Lung Disease. *Genes (Basel)* 10.  
 739 10.3390/genes10030218.
- 740 23. Milone, M.C., and O'Doherty, U. (2018). Clinical use of lentiviral vectors. *Leukemia* 32,  
 741 1529-1541. 10.1038/s41375-018-0106-0.
- 742 24. Kang, H.J., Bartholomae, C.C., Paruzynski, A., Arens, A., Kim, S., Yu, S.S., Hong, Y., Joo,  
 743 C.W., Yoon, N.K., Rhim, J.W., Kim, J.G., et al. (2011). Retroviral gene therapy for X-linked  
 744 chronic granulomatous disease: results from phase I/II trial. *Mol Ther* 19, 2092-2101.  
 745 10.1038/mt.2011.166.
- 746 25. Boztug, K., Schmidt, M., Schwarzer, A., Banerjee, P.P., Diez, I.A., Dewey, R.A., Bohm,  
 747 M., Nowrouzi, A., Ball, C.R., Glimm, H., Naundorf, S., et al. (2010). Stem-cell gene therapy  
 748 for the Wiskott-Aldrich syndrome. *N Engl J Med* 363, 1918-1927.  
 749 10.1056/NEJMoa1003548.
- 750 26. Moratto, D., Giliani, S., Bonfim, C., Mazzolari, E., Fischer, A., Ochs, H.D., Cant, A.J.,  
 751 Thrasher, A.J., Cowan, M.J., Albert, M.H., Small, T., et al. (2011). Long-term outcome and  
 752 lineage-specific chimerism in 194 patients with Wiskott-Aldrich syndrome treated by  
 753 hematopoietic cell transplantation in the period 1980-2009: an international collaborative  
 754 study. *Blood* 118, 1675-1684. 10.1182/blood-2010-11-319376.
- 755 27. Candotti, F., Shaw, K.L., Muul, L., Carbonaro, D., Sokolic, R., Choi, C., Schurman, S.H.,  
 756 Garabedian, E., Kesserwan, C., Jagadeesh, G.J., Fu, P.Y., et al. (2012). Gene therapy for  
 757 adenosine deaminase-deficient severe combined immune deficiency: clinical comparison  
 758 of retroviral vectors and treatment plans. *Blood* 120, 3635-3646. 10.1182/blood-2012-02-  
 759 400937.
- 760 28. Howe, S.J., Mansour, M.R., Schwarzwaelder, K., Bartholomae, C., Hubank, M., Kempski,  
 761 H., Brugman, M.H., Pike-Overzet, K., Chatters, S.J., de Ridder, D., Gilmour, K.C., et al.  
 762 (2008). Insertional mutagenesis combined with acquired somatic mutations causes  
 763 leukemogenesis following gene therapy of SCID-X1 patients. *J Clin Invest* 118, 3143-  
 764 3150. 10.1172/JCI35798.
- 765 29. Strimvelis® (autologous CD34+ enriched cell fraction that contains CD34+ cells  
 766 transduced with retroviral vector that encodes for the human adenosine deaminase [ADA]  
 767 cDNA sequence): first case of lymphoid T cell leukaemia after insertional oncogenesis.  
 768 (2021). <https://www.aifa.gov.it/en/-/nota-informativa-importante-su-strimvelis>.
- 769 30. Holstein, M., Mesa-Nunez, C., Miskey, C., Almarza, E., Poletti, V., Schmeer, M., Grueso,  
 770 E., Ordonez Flores, J.C., Kobelt, D., Walther, W., Aneja, M.K., et al. (2018). Efficient Non-

- 771 viral Gene Delivery into Human Hematopoietic Stem Cells by Minicircle Sleeping Beauty  
 772 Transposon Vectors. *Mol Ther* 26, 1137-1153. 10.1016/j.ymthe.2018.01.012.
- 773 31. Cavazzana, M., Six, E., Lagresle-Peyrou, C., Andre-Schmutz, I., and Hacein-Bey-Abina,  
 774 S. (2016). Gene Therapy for X-Linked Severe Combined Immunodeficiency: Where Do  
 775 We Stand? *Hum Gene Ther* 27, 108-116. 10.1089/hum.2015.137.
- 776 32. Hacein-Bey-Abina, S., Pai, S.Y., Gaspar, H.B., Armant, M., Berry, C.C., Blanche, S.,  
 777 Blesing, J., Blondeau, J., de Boer, H., Buckland, K.F., Caccavelli, L., et al. (2014). A  
 778 modified gamma-retrovirus vector for X-linked severe combined immunodeficiency. *N*  
 779 *Engl J Med* 371, 1407-1417. 10.1056/NEJMoa1404588.
- 780 33. Thornhill, S.I., Schambach, A., Howe, S.J., Ulaganathan, M., Grassman, E., Williams, D.,  
 781 Schiedlmeier, B., Sebire, N.J., Gaspar, H.B., Kinnon, C., Baum, C., et al. (2008). Self-  
 782 inactivating gammaretroviral vectors for gene therapy of X-linked severe combined  
 783 immunodeficiency. *Mol Ther* 16, 590-598. 10.1038/sj.mt.6300393.
- 784 34. De Ravin, S.S., Liu, S., Sweeney, C.L., Brault, J., Whiting-Theobald, N., Ma, M., Liu, T.,  
 785 Choi, U., Lee, J., O'Brien, S.A., Quackenbush, P., et al. (2022). Lentivector cryptic splicing  
 786 mediates increase in CD34+ clones expressing truncated HMGA2 in human X-linked  
 787 severe combined immunodeficiency. *Nat Commun* 13, 3710. 10.1038/s41467-022-31344-  
 788 x.
- 789 35. Brunetti-Pierri, N.E. (2017). *Safety and Efficacy of Gene-Based Therapeutics for Inherited*  
 790 *Disorders* (Springer, 2017).
- 791 36. Hsu, P.D., Lander, E.S., and Zhang, F. (2014). Development and applications of CRISPR-  
 792 Cas9 for genome engineering. *Cell* 157, 1262-1278. 10.1016/j.cell.2014.05.010.
- 793 37. Hendel, A., Bak, R.O., Clark, J.T., Kennedy, A.B., Ryan, D.E., Roy, S., Steinfeld, I.,  
 794 Lunstad, B.D., Kaiser, R.J., Wilkens, A.B., Bacchetta, R., et al. (2015). Chemically  
 795 modified guide RNAs enhance CRISPR-Cas genome editing in human primary cells.  
 796 *Nature biotechnology* 33, 985-989. 10.1038/nbt.3290.
- 797 38. Allen, D., Rosenberg, M., and Hendel, A. (2020). Using Synthetically Engineered Guide  
 798 RNAs to Enhance CRISPR Genome Editing Systems in Mammalian Cells. *Front Genome*  
 799 *Ed* 2, 617910. 10.3389/fgeed.2020.617910.
- 800 39. Chen, X., and Goncalves, M.A. (2016). Engineered Viruses as Genome Editing Devices.  
 801 *Mol Ther* 24, 447-457. 10.1038/mt.2015.164.
- 802 40. Wang, D., Tai, P.W.L., and Gao, G. (2019). Adeno-associated virus vector as a platform  
 803 for gene therapy delivery. *Nat Rev Drug Discov* 18, 358-378. 10.1038/s41573-019-0012-  
 804 9.
- 805 41. Bak, R.O., Dever, D.P., and Porteus, M.H. (2018). CRISPR/Cas9 genome editing in  
 806 human hematopoietic stem cells. *Nat Protoc* 13, 358-376. 10.1038/nprot.2017.143.
- 807 42. Allen, D., Weiss, L.E., Saguy, A., Rosenberg, M., Iancu, O., Matalon, O., Lee, C., Beider,  
 808 K., Nagler, A., Shechtman, Y., and Hendel, A. (2022). High-Throughput Imaging of  
 809 CRISPR- and Recombinant Adeno-Associated Virus-Induced DNA Damage Response in  
 810 Human Hematopoietic Stem and Progenitor Cells. *CRISPR J* 5, 80-94.  
 811 10.1089/crispr.2021.0128.
- 812 43. Bak, R.O., Dever, D.P., Reinisch, A., Cruz Hernandez, D., Majeti, R., and Porteus, M.H.  
 813 (2017). Multiplexed genetic engineering of human hematopoietic stem and progenitor cells  
 814 using CRISPR/Cas9 and AAV6. *Elife* 6. 10.7554/eLife.27873.
- 815 44. Boyd, N., Cartledge, K., Cao, H., Evtimov, V., Pupovac, A., Trounson, A., and Boyd, R.  
 816 (2021). 'Off-the-Shelf' Immunotherapy: Manufacture of CD8(+) T Cells Derived from  
 817 Hematopoietic Stem Cells. *Cells* 10. 10.3390/cells10102631.
- 818 45. Fabio Candotti, J.-P.d.V., Despina Moshous, Anna Villa, Luigi D. Notarangelo. (2020).  
 819 Chapter 7 - Severe combined immune deficiency. [https://doi.org/10.1016/B978-0-12-  
 820 816768-7.00007-7](https://doi.org/10.1016/B978-0-12-816768-7.00007-7).

- 821 46. Fichtner, A.S., Ravens, S., and Prinz, I. (2020). Human gammadelta TCR Repertoires in  
822 Health and Disease. *Cells* 9. 10.3390/cells9040800.
- 823 47. Dudley, E.C., Girardi, M., Owen, M.J., and Hayday, A.C. (1995). Alpha beta and gamma  
824 delta T cells can share a late common precursor. *Curr Biol* 5, 659-669. 10.1016/s0960-  
825 9822(95)00131-x.
- 826 48. Meshaal, S.S., El Hawary, R.E., Abd Elaziz, D.S., Eldash, A., Alkady, R., Lotfy, S.,  
827 Mauracher, A.A., Opitz, L., Pachlopnik Schmid, J., van der Burg, M., Chou, J., et al. (2019).  
828 Phenotypical heterogeneity in RAG-deficient patients from a highly consanguineous  
829 population. *Clin Exp Immunol* 195, 202-212. 10.1111/cei.13222.
- 830 49. Shahzad, M., Siddiqui, R.S., Anwar, I., Chaudhary, S.G., Ali, T., Naseem, M., Ahmed,  
831 T.F., Ahmed, Z., Khurana, S., Ahmed, N., Balusu, R., et al. (2021). Outcomes with CD34-  
832 Selected Stem Cell Boost for Poor Graft Function after Allogeneic Hematopoietic Stem  
833 Cell Transplantation: A Systematic Review and Meta-Analysis. *Transplant Cell Ther* 27,  
834 877 e871-877 e878. 10.1016/j.jtct.2021.07.012.
- 835 50. Ferrari, S., Jacob, A., Beretta, S., Unali, G., Albano, L., Vavassori, V., Cittaro, D.,  
836 Lazarevic, D., Brombin, C., Cugnata, F., Kajaste-Rudnitski, A., et al. (2020). Efficient gene  
837 editing of human long-term hematopoietic stem cells validated by clonal tracking. *Nat*  
838 *Biotechnol* 38, 1298-1308. 10.1038/s41587-020-0551-y.
- 839 51. Wang, J., Exline, C.M., DeClercq, J.J., Llewellyn, G.N., Hayward, S.B., Li, P.W., Shivak,  
840 D.A., Surosky, R.T., Gregory, P.D., Holmes, M.C., and Cannon, P.M. (2015). Homology-  
841 driven genome editing in hematopoietic stem and progenitor cells using ZFN mRNA and  
842 AAV6 donors. *Nature biotechnology* 33, 1256-1263. 10.1038/nbt.3408.
- 843 52. Voit, R.A., Hendel, A., Pruett-Miller, S.M., and Porteus, M.H. (2014). Nuclease-mediated  
844 gene editing by homologous recombination of the human globin locus. *Nucleic Acids Res*  
845 42, 1365-1378. 10.1093/nar/gkt947.
- 846 53. Wang, C.Y., Fang, Y.X., Chen, G.H., Jia, H.J., Zeng, S., He, X.B., Feng, Y., Li, S.J., Jin,  
847 Q.W., Cheng, W.Y., and Jing, Z.Z. (2017). Analysis of the CDR3 length repertoire and the  
848 diversity of T cell receptor alpha and beta chains in swine CD4+ and CD8+ T lymphocytes.  
849 *Mol Med Rep* 16, 75-86. 10.3892/mmr.2017.6601.
- 850 54. Lev, A., Simon, A.J., Trakhtenbrot, L., Goldstein, I., Nagar, M., Stepensky, P., Rechavi,  
851 G., Amarglio, N., and Somech, R. (2012). Characterizing T cells in SCID patients  
852 presenting with reactive or residual T lymphocytes. *Clin Dev Immunol* 2012, 261470.  
853 10.1155/2012/261470.
- 854 55. Serana, F., Chiarini, M., Zanotti, C., Sottini, A., Bertoli, D., Bosio, A., Caimi, L., and Imberti,  
855 L. (2013). Use of V(D)J recombination excision circles to identify T- and B-cell defects and  
856 to monitor the treatment in primary and acquired immunodeficiencies. *J Transl Med* 11,  
857 119. 10.1186/1479-5876-11-119.
- 858 56. Brauer, P.M., Pessach, I.M., Clarke, E., Rowe, J.H., Ott de Bruin, L., Lee, Y.N.,  
859 Dominguez-Brauer, C., Comeau, A.M., Awong, G., Felgentreff, K., Zhang, Y.H., et al.  
860 (2016). Modeling altered T-cell development with induced pluripotent stem cells from  
861 patients with RAG1-dependent immune deficiencies. *Blood* 128, 783-793. 10.1182/blood-  
862 2015-10-676304.
- 863 57. Chang, C.W., Lai, Y.S., Westin, E., Khodadadi-Jamayran, A., Pawlik, K.M., Lamb, L.S.,  
864 Jr., Goldman, F.D., and Townes, T.M. (2015). Modeling Human Severe Combined  
865 Immunodeficiency and Correction by CRISPR/Cas9-Enhanced Gene Targeting. *Cell Rep*  
866 12, 1668-1677. 10.1016/j.celrep.2015.08.013.
- 867 58. Themeli, M., Chhatta, A., Boersma, H., Prins, H.J., Cordes, M., de Wilt, E., Farahani, A.S.,  
868 Vandekerckhove, B., van der Burg, M., Hoeben, R.C., Staal, F.J.T., et al. (2020). iPSC-  
869 Based Modeling of RAG2 Severe Combined Immunodeficiency Reveals Multiple T Cell  
870 Developmental Arrests. *Stem Cell Reports* 14, 300-311. 10.1016/j.stemcr.2019.12.010.

- 871 59. Gardner, C.L., Pavel-Dinu, M., Dobbs, K., Bosticardo, M., Reardon, P.K., Lack, J.,  
872 DeRavin, S.S., Le, K., Bello, E., Pala, F., Delmonte, O.M., et al. (2021). Correction to:  
873 Gene Editing Rescues in Vitro T Cell Development of RAG2-Deficient Induced Pluripotent  
874 Stem Cells in an Artificial Thymic Organoid System. *J Clin Immunol* 41, 863.  
875 10.1007/s10875-021-01030-6.
- 876 60. Canny, M.D., Moatti, N., Wan, L.C.K., Fradet-Turcotte, A., Krasner, D., Mateos-Gomez,  
877 P.A., Zimmermann, M., Orthwein, A., Juang, Y.C., Zhang, W., Noordermeer, S.M., et al.  
878 (2018). Inhibition of 53BP1 favors homology-dependent DNA repair and increases  
879 CRISPR-Cas9 genome-editing efficiency. *Nat Biotechnol* 36, 95-102. 10.1038/nbt.4021.
- 880 61. Liu, M., Rehman, S., Tang, X., Gu, K., Fan, Q., Chen, D., and Ma, W. (2018).  
881 Methodologies for Improving HDR Efficiency. *Front Genet* 9, 691.  
882 10.3389/fgene.2018.00691.
- 883 62. Bifsha, P., Leiding, J.W., Pai, S.Y., Colamartino, A.B.L., Hartog, N., Church, J.A., Oshrine,  
884 B.R., Puck, J.M., Markert, M.L., and Haddad, E. (2020). Diagnostic assay to assist clinical  
885 decisions for unclassified severe combined immune deficiency. *Blood Adv* 4, 2606-2610.  
886 10.1182/bloodadvances.2020001736.
- 887 63. Pavel-Dinu, M., Wiebking, V., Dejene, B.T., Srifa, W., Mantri, S., Nicolas, C.E., Lee, C.,  
888 Bao, G., Kildebeck, E.J., Punjya, N., Sindhu, C., et al. (2019). Author Correction: Gene  
889 correction for SCID-X1 in long-term hematopoietic stem cells. *Nat Commun* 10, 5624.  
890 10.1038/s41467-019-13620-5.
- 891 64. Seet, C.S., He, C., Bethune, M.T., Li, S., Chick, B., Gschwend, E.H., Zhu, Y., Kim, K.,  
892 Kohn, D.B., Baltimore, D., Crooks, G.M., et al. (2017). Generation of mature T cells from  
893 human hematopoietic stem and progenitor cells in artificial thymic organoids. *Nat Methods*  
894 14, 521-530. 10.1038/nmeth.4237.
- 895 65. Bosticardo, M., Pala, F., Calzoni, E., Delmonte, O.M., Dobbs, K., Gardner, C.L., Sacchetti,  
896 N., Kawai, T., Garabedian, E.K., Draper, D., Bergerson, J.R.E., et al. (2020). Artificial  
897 thymic organoids represent a reliable tool to study T-cell differentiation in patients with  
898 severe T-cell lymphopenia. *Blood Adv* 4, 2611-2616.  
899 10.1182/bloodadvances.2020001730.
- 900 66. Somech, R. (2014). Self-reactive and transplacental-acquired maternal T cells in SCID  
901 patients—time to update. *LymphoSign Journal* 2, 47-52. 10.14785/lpsn-2014-0017.
- 902 67. Bertrand, Y., Landais, P., Friedrich, W., Gerritsen, B., Morgan, G., Fath, A., Cavazzana-  
903 Calvo, M., Porta, F., Cant, A., Espanol, T., Muller, S., et al. (1999). Influence of severe  
904 combined immunodeficiency phenotype on the outcome of HLA non-identical, T-cell-  
905 depleted bone marrow transplantation: a retrospective European survey from the  
906 European group for bone marrow transplantation and the European society for  
907 immunodeficiency. *J Pediatr* 134, 740-748. 10.1016/s0022-3476(99)70291-x.
- 908 68. Buckley, R.H., Schiff, S.E., Schiff, R.I., Markert, L., Williams, L.W., Roberts, J.L., Myers,  
909 L.A., and Ward, F.E. (1999). Hematopoietic stem-cell transplantation for the treatment of  
910 severe combined immunodeficiency. *N Engl J Med* 340, 508-516.  
911 10.1056/NEJM199902183400703.
- 912 69. Simonetta, F., Alvarez, M., and Negrin, R.S. (2017). Natural Killer Cells in Graft-versus-  
913 Host-Disease after Allogeneic Hematopoietic Cell Transplantation. *Front Immunol* 8, 465.  
914 10.3389/fimmu.2017.00465.
- 915 70. Hacein-Bey-Abina, S., Von Kalle, C., Schmidt, M., McCormack, M.P., Wulfraat, N.,  
916 Leboulch, P., Lim, A., Osborne, C.S., Pawliuk, R., Morillon, E., Sorensen, R., et al. (2003).  
917 LMO2-associated clonal T cell proliferation in two patients after gene therapy for SCID-  
918 X1. *Science* 302, 415-419. 10.1126/science.1088547.
- 919 71. Woods, N.B., Bottero, V., Schmidt, M., von Kalle, C., and Verma, I.M. (2006). Gene  
920 therapy: therapeutic gene causing lymphoma. *Nature* 440, 1123. 10.1038/4401123a.

- 921 72. Hacein-Bey-Abina, S., Garrigue, A., Wang, G.P., Soulier, J., Lim, A., Morillon, E., Clappier,  
922 E., Caccavelli, L., Delabesse, E., Beldjord, K., Asnafi, V., et al. (2008). Insertional  
923 oncogenesis in 4 patients after retrovirus-mediated gene therapy of SCID-X1. *J Clin Invest*  
924 *118*, 3132-3142. 10.1172/JCI35700.
- 925 73. Miyazaki, K., Watanabe, H., Yoshikawa, G., Chen, K., Hidaka, R., Aitani, Y., Osawa, K.,  
926 Takeda, R., Ochi, Y., Tani-Ichi, S., Uehata, T., et al. (2020). The transcription factor E2A  
927 activates multiple enhancers that drive Rag expression in developing T and B cells. *Sci*  
928 *Immunol* *5*. 10.1126/sciimmunol.abb1455.
- 929 74. Rommel, P.C., Oliveira, T.Y., Nussenzweig, M.C., and Robbiani, D.F. (2017). Correction:  
930 RAG1/2 induces genomic insertions by mobilizing DNA into RAG1/2-independent breaks.  
931 *J Exp Med* *214*, 2167. 10.1084/jem.2016163806092017c.
- 932 75. Pavel-Dinu, M., Gardner, C.L., Nakauchi, Y., Kawai, T., Delmonte, O.M., Palterer, B.,  
933 Bosticardo, M., Pala, F., Viel, S., Malech, H.L., Ghanim, H.Y., et al. (2022). Genetically  
934 Corrected *RAG2*-SCID Human Hematopoietic Stem Cells Restore V(D)J-  
935 Recombinase and Rescue Lymphoid Deficiency. 2022.2007.2012.499831.  
936 10.1101/2022.07.12.499831 %J bioRxiv.
- 937 76. Shapiro, J., Iancu, O., Jacobi, A.M., McNeill, M.S., Turk, R., Rettig, G.R., Amit, I., Toviv-  
938 Recht, A., Yakhini, Z., Behlke, M.A., and Hendel, A. (2020). Increasing CRISPR Efficiency  
939 and Measuring Its Specificity in HSPCs Using a Clinically Relevant System. *Mol Ther*  
940 *Methods Clin Dev* *17*, 1097-1107. 10.1016/j.omtm.2020.04.027.
- 941 77. Amit, I., Iancu, O., Levy-Jurgenson, A., Kurgan, G., McNeill, M.S., Rettig, G.R., Allen, D.,  
942 Breier, D., Ben Haim, N., Wang, Y., Anavy, L., et al. (2021). CRISPECTOR provides  
943 accurate estimation of genome editing translocation and off-target activity from  
944 comparative NGS data. *Nat Commun* *12*, 3042. 10.1038/s41467-021-22417-4.
- 945 78. Fischer, A., and Hacein-Bey-Abina, S. (2020). Gene therapy for severe combined  
946 immunodeficiencies and beyond. *J Exp Med* *217*. 10.1084/jem.20190607.
- 947 79. Hirschhorn, R., Yang, D.R., Puck, J.M., Huie, M.L., Jiang, C.K., and Kurlandsky, L.E.  
948 (1996). Spontaneous in vivo reversion to normal of an inherited mutation in a patient with  
949 adenosine deaminase deficiency. *Nat Genet* *13*, 290-295. 10.1038/ng0796-290.
- 950 80. Stephan, V., Wahn, V., Le Deist, F., Dirksen, U., Broker, B., Muller-Fleckenstein, I.,  
951 Horneff, G., Schroten, H., Fischer, A., and de Saint Basile, G. (1996). Atypical X-linked  
952 severe combined immunodeficiency due to possible spontaneous reversion of the genetic  
953 defect in T cells. *N Engl J Med* *335*, 1563-1567. 10.1056/NEJM199611213352104.
- 954 81. Speckmann, C., Pannicke, U., Wiech, E., Schwarz, K., Fisch, P., Friedrich, W., Niehues,  
955 T., Gilmour, K., Buiting, K., Schlesier, M., Eibel, H., et al. (2008). Clinical and immunologic  
956 consequences of a somatic reversion in a patient with X-linked severe combined  
957 immunodeficiency. *Blood* *112*, 4090-4097. 10.1182/blood-2008-04-153361.
- 958 82. Dvorak, C.C., Long-Boyle, J., Dara, J., Melton, A., Shimano, K.A., Huang, J.N., Puck, J.M.,  
959 Dorsey, M.J., Facchino, J., Chang, C.K., and Cowan, M.J. (2019). Low Exposure Busulfan  
960 Conditioning to Achieve Sufficient Multilineage Chimerism in Patients with Severe  
961 Combined Immunodeficiency. *Biol Blood Marrow Transplant* *25*, 1355-1362.  
962 10.1016/j.bbmt.2019.03.008.
- 963 83. Amit, I., Iancu, O., Levy-Jurgenson, A., Kurgan, G., McNeill, M.S., Rettig, G.R., Allen, D.,  
964 Breier, D., Ben Haim, N., Wang, Y., Anavy, L., et al. (2021). CRISPECTOR provides  
965 accurate estimation of genome editing translocation and off-target activity from  
966 comparative NGS data. *Nature Communications* *12*, 3042. 10.1038/s41467-021-22417-  
967 4.
- 968 84. Hammer, D.A.T.H., P. D. Ryan PAST: Paleontological Statistics software package  
969 for education and data analysis. *Palaeontol. Electron.* *4*, 1–9 (2001).
- 970 85. Lev, A., Simon, A.J., Bareket, M., Bielorai, B., Hutt, D., Amariglio, N., Rechavi, G., and  
971 Somech, R. (2012). The kinetics of early T and B cell immune recovery after bone marrow

972 transplantation in RAG-2-deficient SCID patients. PLoS One 7, e30494.  
973 10.1371/journal.pone.0030494.

974

## 975 List of Figure Captions

976 **Figure 1. Biallelic targeting of SCID-related genes via CRISPR-Cas9/rAAV6 in HD-derived**  
977 **CD34<sup>+</sup> HSPCs. (A)** Schematic representation of *RAG2* disruption donors containing tNGFR or  
978 GFP selectable markers driven by an SFFV promoter and two 400 bp arms of homology for direct  
979 recombination repair (left homologous arm [LHA]; right homologous arm [RHA]). Successful  
980 HDR results in *KI* of the reporter gene approximately 43 bp downstream from the *RAG2* ATG start  
981 codon. *DCLRE1C* and *IL7RA* biallelic editing (not shown here) utilize tdTomato and GFP reporter  
982 genes under the regulation of a SFFV promoter and a BGH polyA sequence. **(B)** FACS approach  
983 for enrichment of biallelic *RAG2* gene-targeted CD34<sup>+</sup> HSPCs 2 days after CRISPR-Cas9 and  
984 rAAV6 editing. Representative HSPC FACS plots of cells transduced with rAAV6 only (*left*) and  
985 cells treated with CRISPR-Cas9 and rAAV6 (*right*) are shown. The double-positive tNGFR<sup>+</sup>/GFP<sup>+</sup>  
986 population indicative of biallelic integration of two different DNA donors was isolated. Gating  
987 determination is based on cells treated with only the rAAV6 vector (*left*) to compensate for the  
988 episomal expression determined to be around 1%. **(C)** GFP and either tNGFR or tdTomato biallelic  
989 targeting frequencies (determined as described above in *Figure 1B*) at *CCR5* (N=10), *RAG2*  
990 (N=11), *DCLRE1C* (N=3), and *IL7RA* loci (N=3). Data are represented as mean ± SEM.

991

992 **Figure 2. SCID modeling using biallelic KO of HD-derived CD34<sup>+</sup> HSPCs in a cell-free IVTD**  
993 **assay. (A)** Flow cytometry analysis of *IL7RA* biallelic KO in IVTD. *IL7RA* biallelic KO cells

994 showed no survival by day 6 of IVTD, based on flow cytometry viability stain out of the double-  
995 positive tdTomato<sup>+</sup>/GFP<sup>+</sup> biallelic enriched population. Double-negative (tdTomato<sup>-</sup>/GFP<sup>-</sup>) cells  
996 showed 100% survival on day 6. Gating was determined by unstained cells. The data represent one  
997 of 3 independent experiments. **(B)** Flow cytometry analysis of T-cell developmental progression.  
998 *Mock*, *CCR5* biallelic KO, *RAG2* biallelic KO, and *DCLRE1C* biallelic KO cells developed normal  
999 expression of early markers of T-cell differentiation (CD7, CD5, and CD1a) upon analysis at 14  
1000 days of IVTD. Following 28 days of IVTD, *Mock* and *CCR5* biallelic KO cells expressed mature  
1001 T-cell markers: CD4, CD8, and CD3, while *RAG2* biallelic KO and *DCLRE1C* biallelic KO cells  
1002 lack CD3 expression. Gating was determined by FMO + isotype controls. The data represent one  
1003 of 3-10 independent repeats (*Mock* [day 14 N=10 and day 28 N=7], *CCR5* KO [day 14 N=10 and  
1004 day 28 N=6], *RAG2* KO [day 14 N=10 and day 28 N=6], and *DCLRE1C* KO [day 14 N=3 and day  
1005 28 N=3]). Cell viability for all samples remained >98% through day 28.

1006

1007 **Figure 3. *RAG2* KI-KO gene correction simulation strategy in HD-derived CD34<sup>+</sup> HSPCs. (A)**  
1008 Schematic representation of *RAG2* correction donor containing diverged codon-optimized *RAG2*  
1009 cDNA and 3' UTR followed by a tNGFR selectable marker under the regulation of a PGK promoter  
1010 and BGH polyA sequence. This is flanked by two 400 bp arms of homology for direct  
1011 recombination repair, labeled LHA and RHA, on the left and right side of the CRISPR cut site,  
1012 respectively. **(B)** Flow cytometry analysis of T-cell developmental progression of *Mock*, *CCR5*  
1013 biallelic KO, *RAG2* biallelic KO, and *RAG2* KI-KO correction simulation cells. All of the groups  
1014 showed normal expression of early markers: CD7, CD5, and CD1a (upon 14 days of IVTD), as  
1015 well as mature T-cell markers: CD4 and CD8 (upon 28 days of IVTD). CD3 expression was  
1016 observed in *Mock*, *CCR5* biallelic KO, and *RAG2* KI-KO correction simulation cells, yet not in

1017 *RAG2* biallelic KO cells. (C) Summary of CD3 expression by *Mock*, *CCR5* biallelic KO, *RAG2*  
1018 biallelic KO, and *RAG2 KI-KO* correction simulation populations at day 28 of IVTD. (N=7, N=6,  
1019 N=6, and N=4, respectively). The data for *Mock*, *CCR5* KO, and *RAG2* KO are taken from *Figure*  
1020 *S3C* and are presented here for comparison to the *RAG2 KI-KO* correction simulation population.  
1021 \*\*  $p < 0.005$  (Mann-Whitney test). Data are represented as mean  $\pm$  SEM.

1022

1023 **Figure 4. Expression of diverged *RAG2* cDNA in *KI-KO* cells leads to the development of**  
1024 **normal TCR repertoire.** (A) Representative tree map depiction of the clonal complexity of the  
1025 TRG deep-sequencing repertoire of differentiated T cells from *Mock*, *CCR5* biallelic KO, and  
1026 *RAG2 KI-KO* correction simulation groups (due to lack of CD3 expression in the *RAG* biallelic  
1027 KO population, sequencing and mapping of the repertoire were impossible). Each square  
1028 represents a unique V-J pair, and the size of each square represents the clone's frequency. (B)  
1029 Shannon and Simpson diversity indices of TRG repertoire on days 14 and 28 of *Mock*, *CCR5*  
1030 biallelic KO, and *RAG2 KI-KO* correction simulation groups. (N=3). Data are represented as mean  
1031  $\pm$  SEM.

1032

1033 **Figure 5. *RAG2* gene correction in *RAG2-SCID* patient-derived CD34<sup>+</sup> HSPCs facilitates**  
1034 **normal T-cell differentiation.** Flow cytometry analysis of T-cell developmental progression, on  
1035 days 14, 28, and 42, of the following cell groups: *Mock*, *RAG2-SCID*, unsorted *RAG2-SCID*  
1036 correction with 12,500 VG/cell, sorted *RAG2-SCID* correction with 12,500 VG/cell, and sorted  
1037 *RAG2-SCID* correction with 6,250 VG/cell. Corrected cells were treated with the same rAAV6  
1038 *RAG2* correction donor depicted in *Figure 3A*. Robust CD3 expression was found on day 28 in all

1039 *RAG2* correction populations, and on day 42 only in the sorted populations. Due to the scarcity of  
 1040 patient-derived sample, N=1 for the *RAG2*-SCID samples and the *Mock* plots are from a  
 1041 representative donor.

1042

1043 **Figure 6. Corrected *RAG2* gene expression in *RAG2*-SCID patient-derived CD34<sup>+</sup> HSPCs**  
 1044 **allows for normal TCR repertoire development.** (A) Representative tree map depiction of the  
 1045 clonal complexity of the TRG deep-sequencing repertoire of differentiated T cells from *Mock*  
 1046 and *RAG2*-SCID correction populations, over the 42 days in the IVTD system (days 14, 28, and  
 1047 42). (B) Shannon and Simpson diversity indices of TRG repertoires on days 14, 28, and 42 of  
 1048 *Mock* and *RAG2*-SCID correction groups (*Mock* [day 14 N=5, day 28 N=4, day 42 N=3]; and  
 1049 *RAG2*-SCID correction groups [day 14, day 28, and day 42 N=1]). Data are represented as mean  
 1050  $\pm$  SEM.

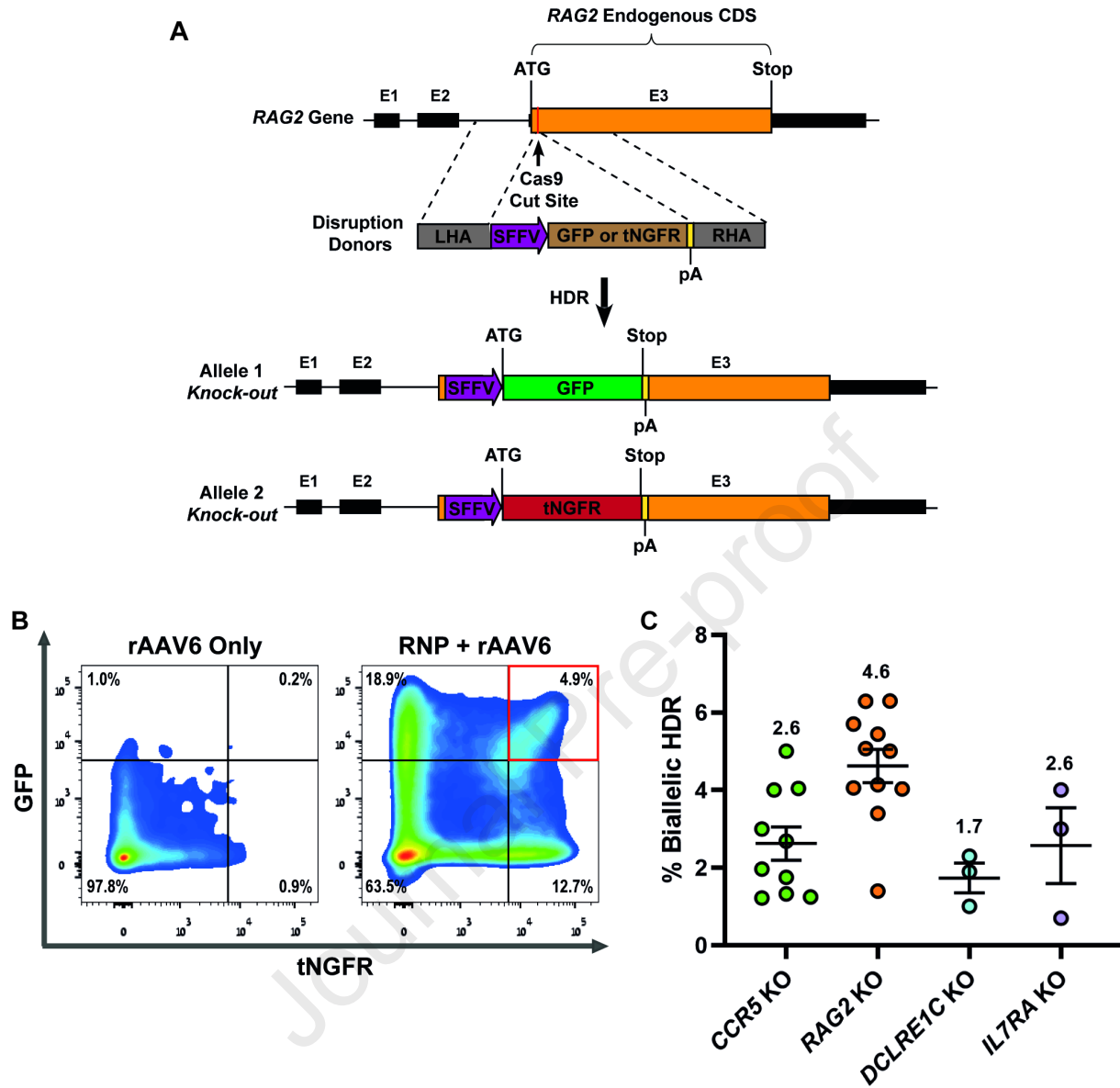
1051

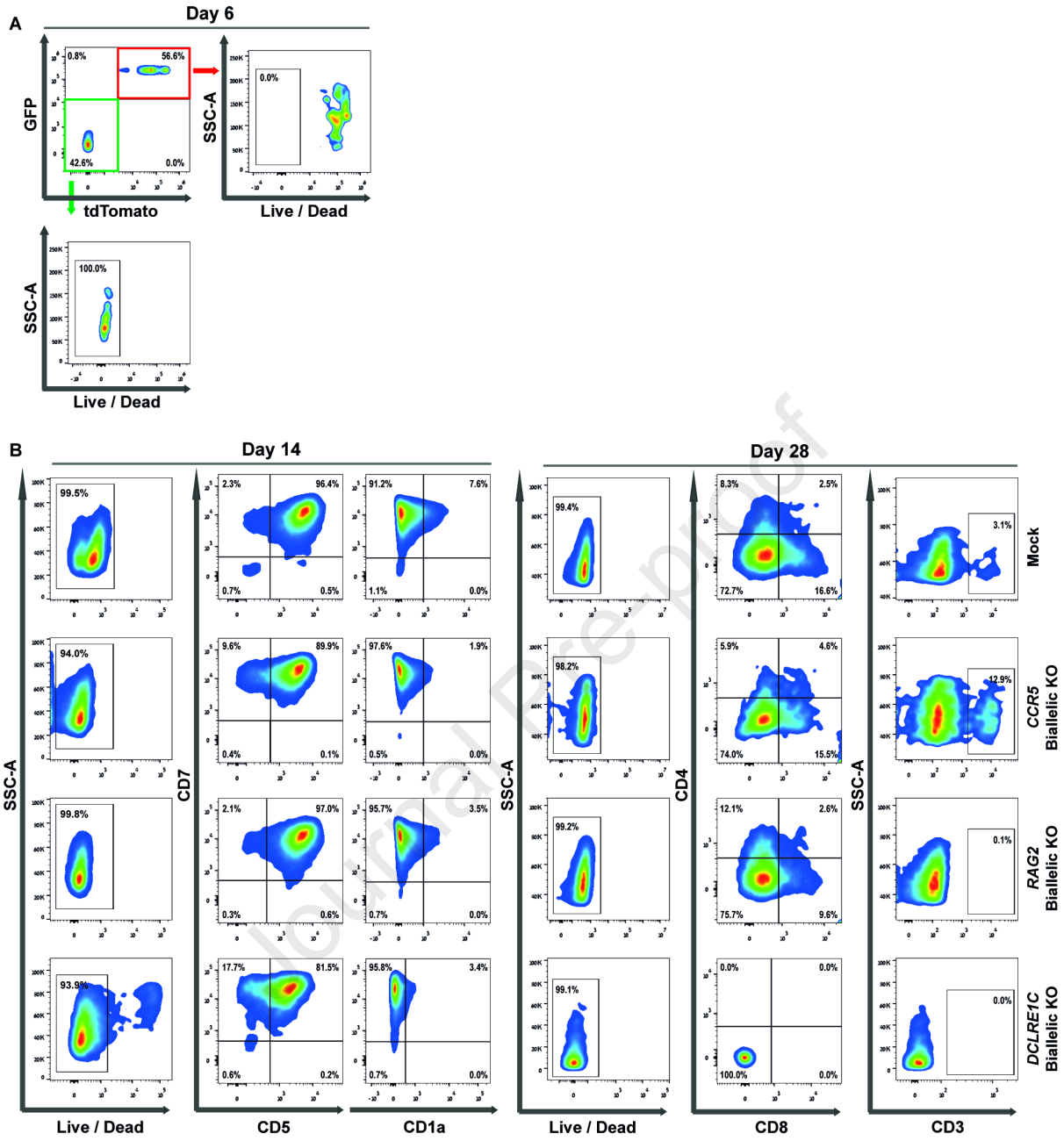
1052 **Table 1. Quantitative PCR analysis of TRECs in *RAG2*-SCID and *RAG2*-SCID correction**  
 1053 **cells over the 42 days in the IVTD system.**

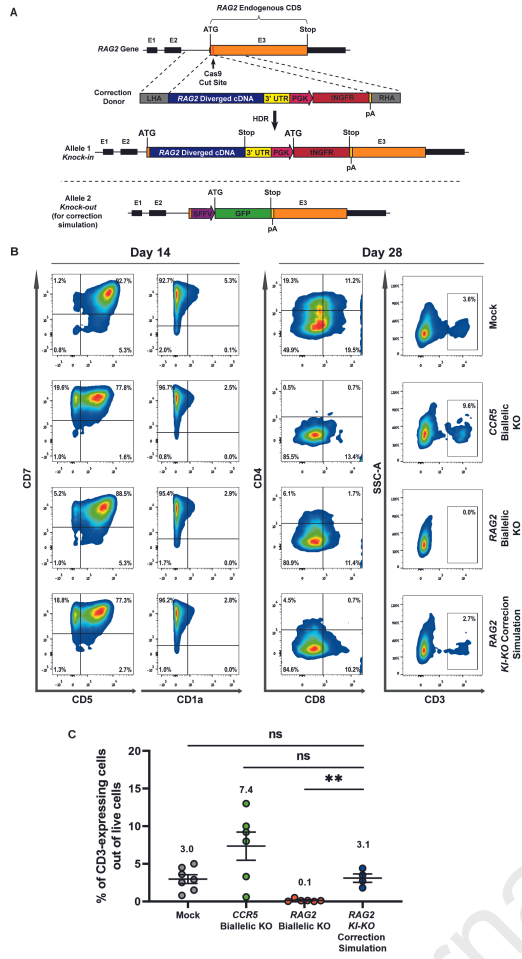
		TREC (copies)	RNase P (average C <sub>T</sub> values)
Day 14	<i>RAG2</i> -SCID	UN	24.9
	Correction <i>RAG2</i> -SCID unsorted	UN	24.8
	Correction <i>RAG2</i> -SCID sorted 12,500 VG/cell	UN	24.3

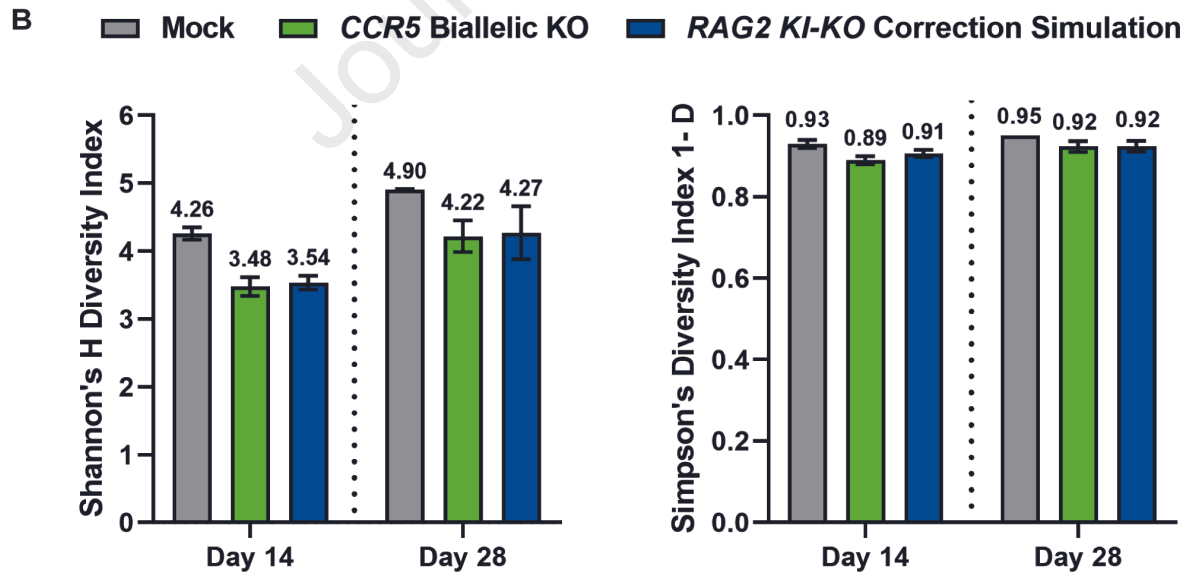
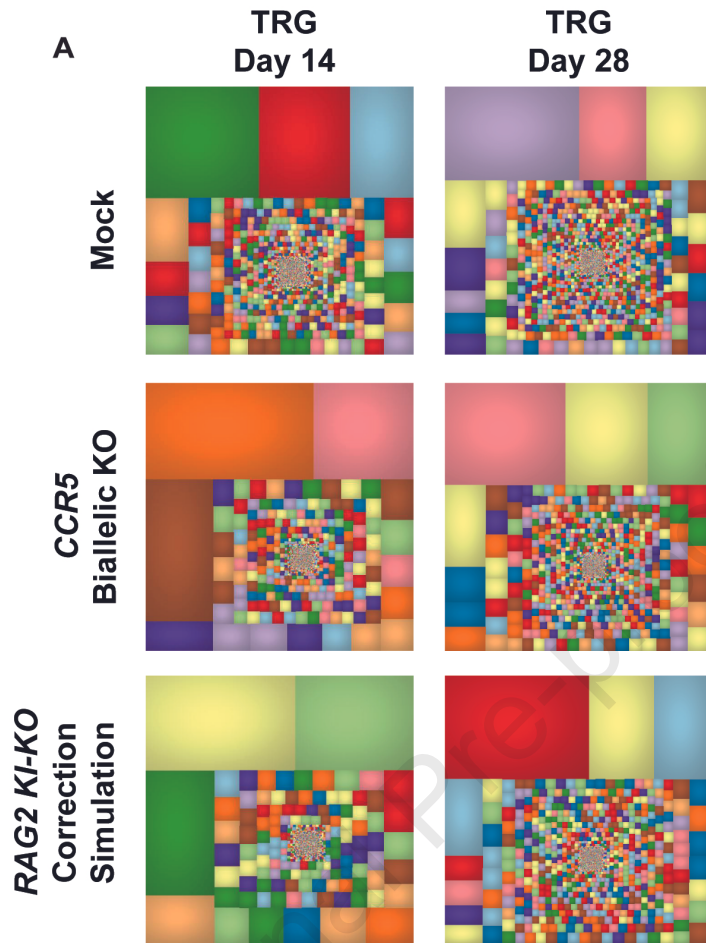
	Correction <i>RAG2</i> -SCID with sorted 6,250 VG/cell	UN	24.7
Day 28	<i>RAG2</i> -SCID	UN	25.1
	Correction <i>RAG2</i> -SCID unsorted	UN	24.7
	Correction <i>RAG2</i> -SCID sorted 12,500 VG/cell	5.4	25.1
	Correction <i>RAG2</i> -SCID sorted 6,250 VG/cell	22.4	24.9
Day 42	<i>RAG2</i> -SCID	UN	24.7
	Correction <i>RAG2</i> -SCID unsorted	UN	24.9
	Correction <i>RAG2</i> -SCID sorted 12,500 VG/cell	8.3	25.6
	Correction <i>RAG2</i> -SCID sorted 6,250 VG/cell	31.5	25.1

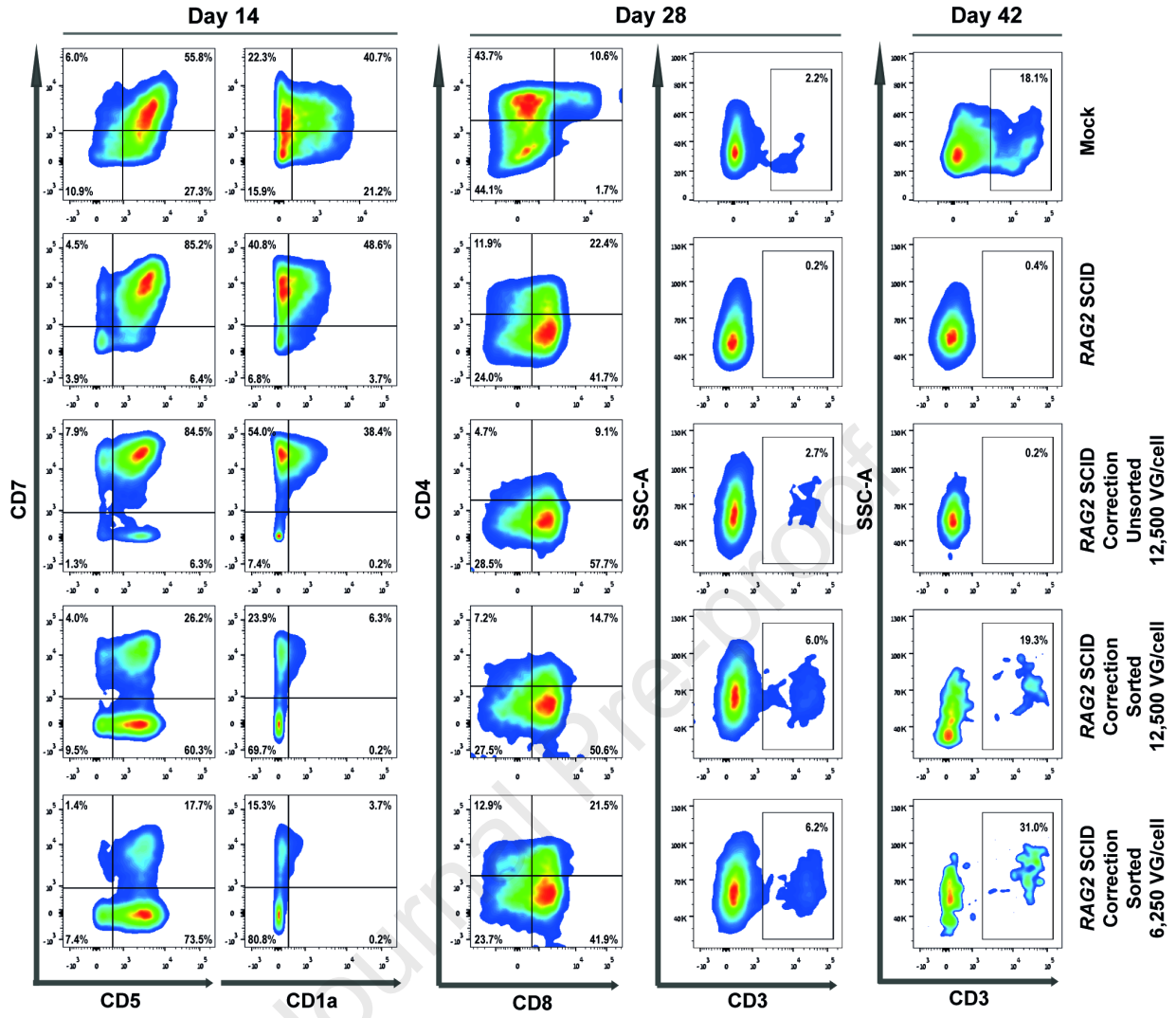
1054 RNase P was used as an internal control for quality of genomic DNA amplification. TRECs were  
1055 detectable solely in the sorted *RAG2*-SCID correction groups on days 28 and 42 in the IVTD  
1056 system. UN = undetermined.

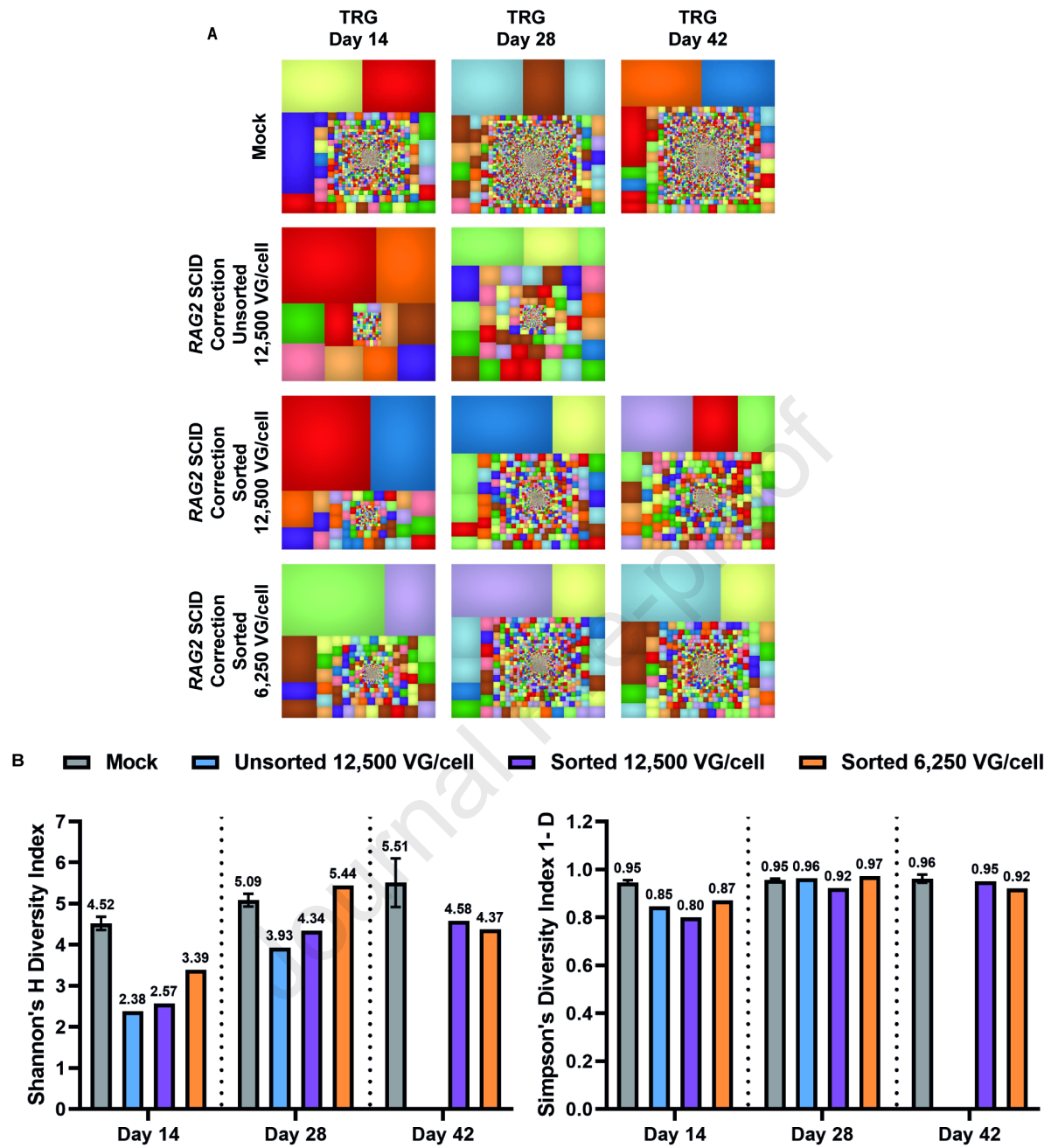












**eTOC Synopsis (50 words)**

We present a platform using CRISPR-Cas9/rAAV6 editing and an *in vitro* T-cell differentiation system where we model SCID disease and present a proof-of-concept gene therapy for treatment of *RAG2*-SCID. This technique eliminates the need for large quantities of patient-derived samples and can be easily translated to other genetic blood disorders.

Journal Pre-proof